Candida auris undergoes adhesin-dependent and -independent cellular aggregation

Chloe Pelletier[1,2,4], **Sophie Shaw**[3,5], **Sakinah Alsayegh**[1], **Alistair J. P. Brown**[2], and **Alexander Lorenz**[1,*]

[1]Institute of Medical Sciences (IMS), University of Aberdeen, Aberdeen, UK

[2]MRC Centre for Medical Mycology, University of Exeter, Exeter, UK

[3]Centre for Genome-Enabled Biology and Medicine (CGEBM), University of Aberdeen, Aberdeen, UK

[4]Present Address: Wellcome Centre for Anti-Infectives Research, School of Life Sciences, University of Dundee, Dundee, UK

[5]Present Address: All Wales Medical Genomics Service, Institute of Medical Genetics, University Hospital of Wales, Cardiff, UK

*Correspondence should be addressed to

Alexander Lorenz

Institute of Medical Sciences (IMS)

University of Aberdeen

Foresterhill

Aberdeen AB25 2ZD

United Kingdom

E-mail: a.lorenz@abdn.ac.uk

ORCIDs: 0000-0002-5581-3442 (CP), 0000-0003-2367-2670 (SS), 0000-0003-1406-4251 (AJPB), 0000-0003-1925-3713 (AL)

Abstract

Candida auris is a fungal pathogen of humans responsible for nosocomial infections with high mortality rates. High levels of resistance to antifungal drugs and environmental persistence mean these infections are difficult to treat and eradicate from a healthcare setting. Understanding the life cycle and the genetics of this fungus underpinning clinically relevant traits, such as antifungal resistance and virulence, is of the utmost importance to develop novel treatments and therapies. Epidemiological and genomic studies have identified five geographical clades (I-V), which display phenotypic and genomic differences. Aggregation of cells, a phenotype primarily of clade III strains, has been linked to reduced virulence in mouse and *Galleria mellonella* infection models. The aggregation phenotype has thus been associated with conferring an advantage for (skin) colonisation rather than for systemic infection. However, strains with different clade affiliations were compared to infer the effects of different morphologies on virulence. This makes it difficult to distinguish morphology-dependent causes from clade-specific or even strain-specific genetic factors. Here, we identify two different types of aggregation: one induced by antifungal treatment which is a result of a cell separation defect; and a second which is controlled by growth conditions and only occurs in strains with the ability to aggregate. The latter aggregation type depends on an ALS-family adhesin which is differentially expressed during aggregation in an aggregative *C. auris* strain. Finally, we demonstrate that macrophages cannot clear aggregates, suggesting that aggregation might after all provide a benefit during systemic infection and could facilitate long-term persistence in the host.

Key words: *Candida auris*, adhesin, cell aggregation, virulence.

Author Summary

Candida auris is a single-celled fungus, a yeast, that can cause severe infections in hospital patients. This fungus is difficult to treat because it is resistant to many antifungal drugs. Therefore, to understand the processes that enhance the virulence of this yeast with a view to developing new treatments. Previous studies have found that *C. auris* can form aggregates, or clumps of cells, which may play a role in how the fungus infects people. In this study, we identified two different types of aggregation in *C. auris*, one triggered by antifungal treatment, and another controlled by growth conditions. This discovery allowed us to study aggregate formation in the same genetic background. In doing so, we found that a certain protein, an ALS-family adhesin, is involved in the aggregation process. Surprisingly, we also discovered that aggregates may promote infection by making it harder for the immune system to clear the yeast. This new understanding could help researchers develop better ways to fight *C. auris* infections.

Introduction

The fungus *Candida auris*, first identified in 2009, has been responsible for outbreaks of infections in hospitals on six continents [1,2]. It has become a global concern due to the high levels of antifungal resistance displayed across the species, its environmental persistence, and its nosocomial transmission [3,4]. The species is divided into 5 clades which have distinct geographic origins and show different levels of intra-clade variations. The 4 main clades, clade I (South Asia), clade II (East Asia), clade III (South Africa), and clade IV (South America) are well documented, whereas only a few isolates of clade V (Iran) have been identified so far [5–7].

In fungi, morphological changes have been linked to gene expression modifications that can impact virulence and pathogenicity [8,9]. For example, the expression of adhesins and proteases are co-regulated alongside the yeast-to-hyphae transition of *Candida albicans* [10]. The yeast *C. auris* typically grows as single ellipsoidal cells, and can form filaments, but not true hyphae, under certain conditions [11,12]. Furthermore, certain *C. auris* strains can form aggregates, which are clumps of cells that cannot be dispersed by chemical or mechanical means and that are thought to be caused by a cell separation defect [13–15]. Cellular aggregation is a phenotype predominantly of clade III strains, but there are also aggregative isolates in clade I and clade II [16–18]. The biological relevance and the genetic requirements for this aggregation morphology are not fully understood yet [19], but some potential factors have recently been identified [14,17,20,21]. Indeed, this kind of cellular behaviour can also be observed in other species of the *Candida haemulonii* complex [21], to which *C. auris* belongs. *C. auris* strains displaying the aggregation phenotype seem to be less virulent, more commonly

88 associated with skin colonisation, have greater biofilm mass, and greater environmental
89 persistence over non-aggregative isolates [16,18,22,23]. A recent study has distinguished
90 two types of aggregation, and has suggested that overexpression of an ALS-family
91 adhesin, caused by copy-number variation of the corresponding locus, is involved in this
92 [17]. So far, a major limitation of studies exploring aggregation has been that aggregative
93 strains are often compared to non-aggregative ones from different clades.

94 Our study has revealed that there are two different kinds of aggregation both of which
95 represent an inducible phenotype. One type of aggregation depends on growth conditions
96 and can only be induced in aggregative strains (mostly clade III strains). The other
97 depends on treatment with sub-inhibitory concentrations of echinocandins (a class of
98 antifungal drugs) and can also be induced in non-aggregative strains. The first type of
99 aggregation is induced by growth in rich medium and repressed in minimal medium. In
100 contrast to media-induced aggregates which are seemingly caused by cells sticking to
101 each other, echinocandin-induced aggregation is characterized by cells that fail to fully
102 separate [15]. Having identified the conditions for media-induced aggregation, we
103 exploited this to elucidate the genetic requirements for this type of aggregation. For this,
104 we performed transcriptomic analysis to identify differentially expressed genes in
105 aggregative and non-aggregative strains grown in rich and minimal medium. We identified
106 a gene with homology to a *C. albicans ALS* gene that is strongly upregulated in the
107 aggregative strain when grown in rich medium. We constructed a deletion mutant of this
108 gene, and the resulting strain lacks the ability to aggregate in rich medium, but still
109 aggregates in response to sub-inhibitory concentrations of echinocandins. We also show
110 that virulence in an invertebrate infection model is affected by pre-infection culture

111 conditions especially for strains with moderate or low virulence. If aggregation is
112 prevented by deletion of the upregulated ALS factor in an aggregative strain, then
113 virulence is moderately reduced. Finally, we used macrophages derived from
114 THP-1 monocytes to demonstrate that aggregates could be difficult for the immune
115 system to clear, and thus could potentially be responsible for persistent infections.

116

117 Results

118 Two distinct types of aggregation

119 The ability to aggregate (or not) has been used to classify strains of *C. auris*, and several
120 studies have reported aggregative capacities for some clinical isolates [15,18,24]. It was
121 thus surprising that, when grown in RPMI-1640, a defined minimal medium, we observed
122 a lack of this phenotype regardless of clade or status as aggregative or non-aggregative
123 strain (Fig 1A). However, we did observe that, if grown in Sabouraud dextrose broth
124 (SabDex), an undefined rich medium, the clade III strain (UACa20) and the clade IV strain
125 (UACa22) did form aggregates alongside single yeast cells, whereas non-aggregative
126 clade I (UACa11) and clade II (UACa83) strains did not show any clumping of cells (Fig
127 1A). The inability of this clade I isolate to aggregate, as well as the aggregative ability of
128 the clade III strain, we used in this study, agreed with previous observations [16].

129 We also found that, after growth in SabDex, aggregation was affected by the chemical
130 composition of the liquid used to resuspend the cells. Aggregating cultures retained
131 aggregation when resuspended in 1× PBS (phosphate-buffered saline), but aggregation
132 was greatly reduced when cells were resuspended in ddH_2O (Fig 1B). Interestingly, cells

133 that were dis-aggregated in ddH_2O, immediately re-aggregated when they were then
134 resuspended in 1× PBS (Fig 1B). Non-aggregative strains remained as single cells
135 regardless of suspension liquid (Fig 1B). This strongly indicates that a cell wall component
136 that remains present regardless of the change in suspension liquid is associated with
137 aggregation.

138 It has been reported that *C. auris* strains aggregate in response to sub-inhibitory
139 concentrations of two classes of antifungals, azoles, and echinocandins [15,16]. We
140 focused on two echinocandins, caspofungin (CSP) and micafungin (MFG) as these drugs
141 are used preferentially in the clinical setting to treat *C. auris* infections (CDC Guidelines,
142 PHE Guidlines). E-test strips were used to determine minimum inhibitory concentrations
143 (MICs) for the strains tested (Table S1). Growth was not completely abolished at any
144 concentration of CSP but was clearly diminished above a certain concentration which we
145 recorded as the MIC_{90} value (Table S1, Fig S1). Growth in the presence of MFG was
146 abolished above 0.094 mg/L for clade I strains UACa11 and UACa25 (Table S1, Fig S2).
147 However, for the clade III strains (UACa10 and UACa20) MIC_{90}s of 0.094 mg/L and 0.064
148 mg/L, respectively, were determined as residual background growth was observed above
149 these concentrations (Table S1, Fig S2). Therefore, 32 mg/L CSP and 0.075 mg/L MFG
150 were chosen as subinhibitory concentrations.

151 Echinocandin-induced aggregation experiments were performed in RPMI-1640 to avoid
152 clade III strains forming media-induced aggregates. Indeed, both the aggregative clade
153 III strain (UACa20) and the non-aggregative clade I strain (UACa11) formed aggregates
154 when grown in RPMI-1640 containing either 32mg/L CSP or 0.075 mg/L MFG (Fig 2A-B),
155 but not in the presence of the DMSO vehicle (Fig S3). These aggregates did not disperse

156 when cells were resuspended in ddH_2O, indicating that antifungal-induced aggregation
157 differs from media-induced aggregation (Figs 1B, 2A-B). This difference was also
158 noticeable when looking at the liquid cultures. After 5 minutes without agitation there was
159 noticeable sedimentation of the media-induced aggregates in the aggregative UACa20
160 (clade III) strain not seen in any of the other cultures (Fig 2C). However, both the non-
161 aggregative UACa11 (clade I) isolate and the aggregative UACa20 (clade III) strain
162 largely remained in suspension when echinocandin-dependent aggregates were formed
163 (Fig 2C). Neither media- nor echinocandin-induced aggregation was reflected in an
164 altered colony morphology on solid medium (Fig 2D).

165 The capacity of media-induced aggregates to dissociate and reform depending on the
166 suspension liquid, suggests the involvement of a component of (or associated with) the
167 cell wall, whereas the stability of antifungal-induced aggregates is consistent with a cell
168 separation defect [15]. To explore these phenotypes in more detail, we used calcofluor
169 white (CFW) to stain total cell wall chitin on paraformaldehyde-fixed cells. Media-induced
170 aggregates contained a mix of larger rounded cells marked with multiple bud scars
171 alongside smaller ellipsoidal cells (Fig 3A). It was also noted that the media-induced
172 aggregates started to fall apart when proteinase K treatment was used during preparation,
173 causing aggregates to spread out across glass slides during preparation for microscopy.
174 No pressure was applied during preparation as a hard-set mounting medium was used.
175 In contrast, echinocandin-induced aggregates appeared to grow from a small cluster of
176 cells with daughter cells emanating from a central point (Fig 3B). These tight clusters of
177 cells retained their shape during microscopy even after treatment with proteinase K. The
178 daughter cells appeared to remain attached to their mothers indicating a cytokinesis

179 defect similar to rapamycin-treated cells [25]. A lack of obvious bud scars on cells at the
180 edge of clusters corroborates this interpretation (Fig 3B) [25].

181 To better understand whether antifungal-induced aggregation was due to a cell
182 separation defect, confocal microscopy was used to visualize aggregates in three
183 dimensions. UACa20 (clade III) cells grown in SabDex were double-stained with CFW
184 (chitin) and Concanavalin A (ConA) (cell wall mannan). Media-induced aggregates
185 displayed an intact chitin cell wall that was completely covered by mannan (Fig 3C, red
186 arrows). Only small budding cells lacked the mannan outer cell wall layer between mother
187 and daughter cells (Fig 3C, white arrows). In contrast, cells in antifungal-induced
188 aggregates had a chitin layer completely surrounding them, but there was a lack of a
189 mannan layer where cells were closely juxtaposed (Fig 3D, white arrows), similar to small
190 budding cells in media-induced aggregates. Again, this is consistent with the idea that
191 antifungal-induced aggregation is the result of a cell separation defect, as previously
192 suggested [13–15,17].

193 During the preparation of cells for microscopy we noted that there was a lack of cohesion
194 of media-induced aggregates as well as loss of aggregation after treatment with
195 proteinase K for 1 hour at 50 °C. This was never observed for echinocandin-induced
196 aggregates. To quantify this observation, aggregates were counted using a
197 haemocytometer, and 1×10^6 aggregates were heated at 50 °C for 1 hour with or without
198 12.5 μg of proteinase K. The $\log_2$-fold change of aggregates remaining after treatment
199 was determined relative to number of aggregates before treatment. As predicted, the
200 number of media-induced aggregates showed a significant decrease when proteinase K
201 was present. For UACa20 (clade III), there was a significant ~15-fold decrease ($p = 0.03$,

202 independent samples t-test), and UACa10 (clade III) showed a significant ~28-fold
203 decrease ($p < 0.001$, independent samples t-test) in aggregates after treatment with
204 proteinase K (Fig 4A). These results are consistent with observations by others [17,21],
205 and suggest that the cell wall component involved in media-induced aggregation is not
206 perturbed by temperatures up to 50 °C. Neither CSP- nor MFG-induced aggregates were
207 significantly reduced by proteinase K treatment (Fig 4B-C).

208 Based on these observations, to semantically distinguish these phenotypes, we propose
209 that media-induced aggregation is henceforth referred to as "aggregation", whereas
210 aggregation caused by a cell separation defect is called "clustering". We focused on
211 aggregation induced by growth conditions to understand why this phenotype only occurs
212 in some isolates of *C. auris* and what the biological relevance of this phenotype might be.

213 **Media-induced aggregation is not correlated with cell wall ultrastructure**

214 Dispersion of aggregates by proteinase K suggested that a proteinaceous cell wall
215 component is involved in media-induced aggregation. To rule out other cell wall
216 ultrastructure changes and a potentially obscure cell separation defect, transmission
217 electron microscopy (TEM) was performed. Cells were grown in either RPMI-1640 or
218 SabDex before high-pressure freezing fixation without washing. No noticeable differences
219 in the cell wall ultra-structure were observed between conditions for all strains regardless
220 of the growth conditions (Fig 5A).

221 The diameters of the inner and outer cell walls for 30 cells from each condition were
222 measured. The diameter of the inner cell wall of non-aggregative strain UACa25 (clade I)
223 showed a significant increase of 21 nm ($p < 0.001$, independent samples t-test) when
224 grown in SabDex compared to RPMI-1640, but there was no significant difference for

225 UACa11 (clade I), a second non-aggregative strain. Aggregative clade III strains UACa6
226 and UACa20 grown in SabDex had significantly thicker inner cell walls by 20 nm ($p <$
227 0.001, independent samples t-test) and 25 nm ($p < 0.001$ independent samples t-test),
228 respectively, than when grown in RPMI-1640 (Fig 5A). The mannan fibrils (outer cell wall)
229 of UACa25 (clade I) were significantly longer by 18 nm ($p < 0.001$, independent samples
230 t-test) when grown in SabDex compared to RPMI-1640 (Fig 5B). While UACa20 (clade
231 III) grown in SabDex had slightly longer mannan fibrils by 4 nm ($p = 0.029$, independent
232 samples t-test) compared to when grown RPMI-1640. There were no significant
233 differences of outer cell wall diameters for UACa6 (clade III) and UACa11 (clade I).
234 Although there were differences in inner and outer cell wall thickness between the two
235 growth conditions, there was no clear trend which separated aggregative from non-
236 aggregative isolates.

237 **Transcriptomic analysis identifies clade-specific and aggregation-specific**
238 **differentially expressed genes**

239 We had shown that the aggregation phenotype is inducible in aggregative isolates, which
240 mostly belong to clade III (Fig 1A). Therefore, we opted to exploit this by using RNA-seq
241 to characterize genetic requirements and identify drivers of aggregation in UACa20 (clade
242 III) compared to the non-aggregative clade I strain UACa11. We compared differentially
243 expressed genes (DEGs) between growth in RPMI-1640 and SabDex for both strains,
244 and then compared these DEGs between UACa20 (clade III) and UACa11 (clade I) to
245 identify changes in transcription that may be important for aggregation. Differential
246 expression analysis was carried out by pairwise comparison between each sample group
247 each consisting of three independent samples, which allowed identification of DEGs

248 between growth in SabDex compared to RPMI-1640 with genes being identified from the
249 *C. auris* B11221 genome (UACa20 in this study). For UACa11 (clade I), from a total of
250 5,419 candidate open reading frames 3,191 significant DEGs at FDR < 0.05 were
251 identified (Fig 6A). For UACa20 (clade III), from a total of 5,431 candidates 3,393
252 significant DEGs at FDR < 0.05 were determined (Fig 6B). There were 997 common
253 DEGs between the two strains. These genes may be involved in adapting to growth under
254 the two different media conditions (Fig 6C), and hence were excluded from further
255 analysis. Genes with a log2FC difference greater than 2 between UACa20 (clade III) and
256 UACa11 (clade I) but with increased expression in SabDex in both strains were identified
257 (Table S2). Furthermore, we also extracted genes that displayed expression in opposite
258 directions between UACa11 (clade I) and UACa20 (clade III) when grown in SabDex
259 (Table S3). Ultimately, we decided to focus on genes that were uniquely upregulated in
260 the aggregative UACa20 strain compared to the non-aggregative UACa11 strain during
261 growth in SabDex, as we hypothesized that this would lead us to a positive effector of
262 aggregation. UACa11 (clade I) had 505 unique DEGs during growth in SabDex, while
263 UACa20 (clade III) had 658 unique DEGs (Fig 6C).

264 The top 10 unique genes upregulated during SabDex growth for UACa11 (clade I) and
265 UACa20 (clade III) are shown in Tables S4 and S5, respectively. To understand their
266 possible gene functions the *C. albicans* homologues were identified. First, the B11221
267 nucleotide sequence of each of those genes (Tables S4-S5) was BLAST-searched
268 against the B8441 genome and the corresponding gene/systematic ID names in B8441
269 were obtained. The B8441 gene identifiers were then used in the batch-download feature
270 of the *Candida* genome database (http://www.candidagenome.org) to identify

271 orthologues and best hits in the *C. albicans* SC5314 genome. The best hit in UACa11
272 (clade I) (Table S4) and the second-best hit in UACa20 (clade III) (Table S4) have been
273 identified as homologous to *C. albicans ALS4*. However, these represent two different *C.*
274 *auris* genes and they show differential regulation in regard to growth media, which was
275 unexpected. ALS (Agglutinin-Like Sequence)-containing proteins form a family of nine
276 adhesins in *C. albicans* with various roles including adherence to plastic and host tissues
277 [26]. *C. auris* genomes seem to contain three separate loci that harbour an Agglutinin-
278 Like Sequence (ALS) [27,28]. Representatives from clade II miss one of the *ALS*-family
279 genes, and in some strains a particular *ALS* gene might be amplified (copy-number
280 variation) [17,28]. Intriguingly, one of these factors (B9J08_004112, XP_028889036) has
281 mostly been studied, and varyingly touted as the ortholog to *C. albicans* Als3 [29], Als4
282 [17,28], or Als5 [22]. This is confusing, and as ALS factors in *C. albicans* have distinct
283 roles and different expression patterns, it is imprudent to assign orthology in *C. auris* when
284 function and gene expression cues have not been established in this species. Indeed,
285 phylogenetic analysis indicates that ALS-family members cluster by species and not by a
286 particular type of ALS from different species [28], this also seems to be the case for Hyr/Iff-
287 like adhesins [30]. To prevent further confusion, we follow the solution proposed by
288 O'Meara and colleagues [31] to use the unique number in the systematic ID as gene
289 number. And therefore, B9J08_004112/XP_028889036 should be called Agglutinin-Like
290 Sequence 4112 (*ALS4112*/Als4112), B9J08_002582 *ALS2582*, and B9J08_004498
291 *ALS4498*. This nomenclature should avoid potential confusion with ALS-type proteins
292 from other species where exact relationships are hard to establish.

293 **Als4112 is necessary for aggregation**

294 The *C. albicans* ALS-family proteins are found on the cell surface, play prominent roles
295 in adhesion to host tissues and other surfaces, and are important for virulence [26,32,33].
296 As media-induced aggregation is likely caused by a cell surface protein and *ALS4112*
297 displays differential expression during SabDex and aggregative growth in UACa20 (clade
298 III), this gene was taken forward as a candidate for potentially playing a role in
299 aggregation. We attempted to generate a clean *als4112* deletion in the aggregative strain
300 UACa20 (clade III). Unfortunately, due to the difficulties in the genetic manipulation of *C.*
301 *auris* [12,19,34], the one mutant strain we obtained harboured an approximate 21.3 kb
302 deletion encompassing the *ALS4112* locus and genes CJI97_004175, CJI97_004176,
303 CJI97_004177, CJI97_004178, CJI97_004179, CJI97_004180, as determined by inverse
304 PCR (Fig S4). We proceeded with this mutant as the additional genes deleted were not
305 present as DEGs in our RNA-seq dataset and are, therefore, not thought to play a role in
306 aggregation; the *als4112* mutant strain also did not display an obvious growth defect. This
307 *als4112* mutant failed to aggregate after 24 hours of growth in SabDex but did still cluster
308 upon exposure to 0.075 mg/L MFG (Fig 7A). This reinforces the idea that there are two
309 distinct types of aggregation, because the same type of cell separation defect is observed
310 in echinocandin-induced clustering in the wild-type clade III UACa20 strain, as well as in
311 the *als4112* mutant made in the same background (Figs 3D and 7B). Thus, *ALS4112*
312 appears to be a key genetic requirement for media-induced aggregation but not for
313 echinocandin-mediated clustering.

314 **Virulence depends on growth conditions of cells before inoculation**

315 There are mixed reports regarding the impact of aggregation on virulence in *Galleria*
316 *mellonella* and mouse infection models, with some studies showing reduced virulence of
317 aggregative strains in contrast to others observing no such a correlation [13,18,35].
318 Indeed, an infection study conducted in neutropenic mice found that there was no obvious
319 association of a given strain's virulence with either its aggregative capacity or it being
320 isolated from the blood stream [18]. Given that in other *Candida* species, such as *C.*
321 *albicans*, virulence can be influenced by cellular morphology [10], we decided to
322 investigate whether virulence was impacted by the aggregation morphology or was
323 isolate-dependent using an *in vivo G. mellonella* infection assay. Fungal cells were grown
324 in either RPMI-1640 as single cells or pre-grown in SabDex inducing the aggregation
325 phenotype in aggregative isolates UACa20 (clade III), UACa6 (clade III), and UACa23
326 (clade IV) while non-aggregative isolates UACa11 (clade I), UACa25 (clade I), and
327 UACa83 (clade II) remained as single cells, before being injected into the moth larvae.

328 All isolates, with the exception of UACa25 (clade I), showed a significant ($p < 0.05$)
329 increase in killing regardless of their ability to aggregate when grown in SabDex, rather
330 than RPMI-1640, before inoculation (Fig 8A-F). This suggests that virulence does not
331 depend directly on the ability to aggregate, but is more likely driven by more complex
332 strain-specific traits influenced by pre-inoculation culture conditions. Being grown in rich
333 medium (SabDex) before inoculation in particular boosts pathogenicity of strains with low
334 to moderate virulence (Fig 8C-F), whereas the two clade I strains receive comparatively
335 little benefit (Fig 8A-B). Indeed, also in *C. albicans* growth conditions influence virulence
336 in invertebrate and vertebrate models of infection [36,37].

337 As the *als4112* deletion strain in the UACa20 background allowed us to directly assess
338 whether aggregation impacts virulence. We also compared the wild-type UACa20 isolate
339 with UACa177 in the *Galleria* infection model after growing these strains in SabDex,
340 where UACa20 aggregates and UACa177 does not. The aggregating wild-type UACa20
341 isolate was moderately, but significantly, more virulent than the non-aggregating
342 *als4112*Δ mutant strain UACa177 (Figs 8G). This suggests that ALS-dependent
343 aggregation has a positive effect on virulence rather than a negative one as previously
344 thought [13].

345 **Aggregates are not cleared by macrophages**

346 Aggregates have been reported in tissue from sacrificed animals [18]. Given the bulky
347 nature of aggregates, we wanted to understand how they would interact with
348 macrophages. THP-1 monocytes were differentiated into macrophages with 200 nM
349 phorbol 12-myristate 13-acetate (PMA) and co-cultured at a multiplicity of infection (MOI)
350 of 1:3 with UACa20 (clade III) cells, which were either grown in SabDex, RPMI-1640,
351 RPMI-1640 containing 0.001% DMSO, or RPMI-1640 containing 0.075 mg/L MFG and
352 0.001% DMSO. Cells were washed and added to CO_2-independent medium for co-
353 culture. Aggregates were counted as one unit for MOI; because cell uptake by
354 macrophages was not quantified, we do not consider this an issue. For cells grown in
355 RPMI-1640 or RPMI-1640 containing 0.001% DMSO, there was no noticeable defect in
356 uptake of single yeast cells (Videos V1 & V2). When presented with media-induced
357 aggregates (Fig 9A, Video V3) or MFG induced clusters (Fig 9B, Video V4) macrophages
358 struggled to engulf the mass of fungal cells with fungal growth occurring at the site not
359 occupied by the macrophage. Media-induced aggregation is not complete, as it produces

360 a heterogenous population of single cells and large aggregates. The single yeast cells
361 under these co-culture conditions are readily taken up by macrophages (Video V5). This
362 indicates that there is no issue with sensing the *C. auris* cells growing under aggregating
363 conditions but that the ability of macrophages to clear the fungal aggregates is dampened.
364 Aggregation and clustering could potentially be causes for long-term persistence of fungal
365 cells in the host and thereby contribute to increased virulence.

366

367 **Discussion**

368 Here, we show that aggregative *C. auris* strains, usually belonging to clade III, only
369 aggregate when grown in a rich medium, such as SabDex or YPD (Fig 1A). This
370 aggregation phenotype is repressed in a minimal medium, such as RPMI-1640, in which
371 aggregative strains grow as single-celled yeasts, like non-aggregative strains (Fig 1A). A
372 second type of aggregation, which we suggest calling “clustering”, was seen when cells
373 were exposed to sub-inhibitory concentrations of echinocandins. This clustering can be
374 induced in aggregative and non-aggregative strains (Fig 2). Such changes in
375 morphological phenotype in *C. auris,* which are triggered by environmental cues, are likely
376 biologically relevant. Similar morphological transitions are observed in other *Candida*
377 species where the switches are often associated with cell stress, such as increased
378 temperature or lack of nutrients [38,39]. SabDex is a rich undefined medium, so the switch
379 of aggregative strains to grow as aggregates suggests that either rich medium is causing
380 some cellular stress or contains specific chemical triggers for such a switch. Indeed, our
381 work highlights the importance of selecting appropriate growth conditions for
382 experimentation with *C. auris,* especially when the aggregation phenotype is to be

383 dissected. Hence, publicly available data from previous work should be reanalysed
384 cautiously [15], as effects of media-induced aggregation and antifungal-induced
385 clustering could potentially confound each other.

386 It was originally assumed that aggregates in *C. auris* formed due to a lack of cell
387 separation [13]. Indeed, some genetic requirements for this type of cell clustering have
388 been identified by elegant forward genetic screening [14,40]. We only saw this particular
389 phenotype when we exposed *C. auris* strains to echinocandins, and this did not happen
390 when *C. auris* clade III strains were grown in rich media (Fig 1A & 3). However, Bing *et*
391 *al*. (2023) characterized a clinical *C. auris* clade I isolate that forms clusters via a cell
392 separation defect, which seems to be inherent to this particular strain [17]. It will be
393 interesting to assess whether clustering in this strain can be modulated by growth
394 condition or is exacerbated by treatment with echinocandins. In the same study [17], a *C.*
395 *auris* clade III strain was shown to undergo proteinase-sensitive aggregation which is
396 associated with overexpression of an ALS-type adhesin (B9J08_004112). For reasons
397 outlined above, we refer to B9J08_004112 as *ALS4112*. Overexpression of Als4112 (Bing
398 *et al*. call it Als4 [17]) in some clinical *C.auris* clade III isolates is apparently caused by
399 copy-number variation of that gene apparently linked to adherence and biofilm forming
400 capability [17]. Copy-number variation and induced gene expression levels also neatly
401 explain our observation that a change in media provokes aggregation. In such a scenario,
402 an aggregative strain expresses Als4112 at low levels when grown in minimal medium
403 (RPMI-1640) but has a high-enough copy number of *ALS4112* [17] to produce sufficient
404 protein molecules to enable aggregation once expression is induced. Here, we find that
405 the non-aggregative UACa11 clade I strain does not upregulate expression of *ALS4112*

406 when grown in SabDex but a different *ALS* gene, *ALS2582* (B9J08_002582). Als2582 at
407 861 amino acids is considerably smaller than Als4112 (1804 amino acids). Our data
408 suggest that Als2582 does not drive aggregation, as UACa11 (clade I) does not form
409 aggregates. Whether this particular adhesin is involved in biofilm formation, adherence to
410 host cells, or adherence to other surfaces (medical equipment) remains to be tested.
411 Indeed, a recently identified *C. auris*-specific adhesin, Scf1, contributes to virulence by
412 promoting adhesion to both biological and abiotic surfaces [31].

413 We show that antifungal treatment causes a cell separation defect which leads to the
414 formation of cell clusters, and that this phenotype is independent of the ability to
415 aggregate in response to the growth media, which has been assumed to be the typical
416 aggregation phenotype [13,17]. Although this is an important distinction to make, both
417 forms of aggregation are apparently hard to clear by the immune system, as our
418 coincubation experiments with macrophages show (Fig 9, Videos V1-V5). Further studies
419 will be needed to fully understand the implications of media-induced aggregation and
420 antifungal-mediated clustering on clinical treatment. The differences in aggregation types
421 might also explain the varying results linking biofilm formation and aggregation ability in
422 separate studies [17,22,23].

423 We focused our attention on media-induced aggregation as there is mounting evidence
424 that aggregation of this type is associated with increased biofilm formation and adherence
425 [17]. Given the importance of the cell wall in cell-cell interactions we examined the cell
426 wall ultrastructure comparing *C. auris* cells from different strains grown in RPMI-1640 and
427 SabDex (Fig 5). TEM showed a lack of obvious differences indicating that cell wall
428 mannans are not notably remodelled between aggregated and single cells, supporting

429 the hypothesis of a protein which is not a bulk component of the cell wall mediating media-
430 induced aggregation. We observed moderate, but significant differences in inner cell wall
431 thickness and mannan fibril length between growth condition in some isolates, but these
432 were strain-specific and not associated with a particular clade or the ability to aggregate.

433 Transcriptomic analysis demonstrated large differences in gene expression between
434 strains of different clades, with 505 DEGs unique to UACa11 (clade I) and 653 DEGs
435 unique to UACa20 (clade III). Of interest to us was that two distinct *ALS* genes were
436 differentially expressed indicating that different ALS-type adhesins might have separate
437 roles [16]. We produced an *als4112* null mutant with some difficulty despite trying multiple
438 techniques, including CRISPR-Cas9-targeted mutation [14]; this might have been
439 aggravated by copy-number variation at the locus [17]. Our *als4112* mutant unfortunately
440 is not a clean deletion, but the region removed does not contain differentially expressed
441 genes identified in our RNA-seq data (Fig S4). Therefore, these genes may not play a
442 role in aggregation and this mutant was thus used for analysis. The results suggest that
443 Als4112 is involved in media-induced aggregation as *als4112* cells formed no aggregates
444 after 24 hours of growth in SabDex. A different mechanism underpins antifungal-induced
445 clustering, as this phenotype was unaffected in *als4112*Δ cells (Figs 2 & 7). This result
446 corroborates the work by Bing *et al.* (2003) where they showed that overexpression of
447 Als4112 induced the aggregation phenotype in non-aggregating strains and that clinical
448 isolates lacking a fully functional Als4112 do not aggregate [17].

449 The *G. mellonella* infection model has been useful for comparing the pathogenicity of *C.*
450 *auris* strains [35]. Intriguingly, we show that the choice of growth medium for the inoculum
451 has a significant impact on the outcome (Fig 8A-F). Cells grown in SabDex are more

452 virulent than those grown in RPMI-1640 for all strains tested except one, the non-
453 aggregative clade I strain UACa25. Further testing with a lower starting inoculum of
454 UACa25 (clade I) would rule out a toxic shock phenomenon that could be caused by
455 UACa25 (clade I) having a higher overall virulence compared to other strains (Fig 8A-F).
456 This demonstrates the importance of experimental design and of detailed reporting of
457 experimental conditions to enable a valid comparison across published results.
458 Importantly, when the contribution of aggregation to virulence was directly tested by
459 comparing the wild-type UACa20 isolate to the *als4112*Δ mutant, wild-type infection
460 reduced survival among *G. mellonella* larvae significantly (Fig 8G).

461 Another difficulty working with aggregation is to correctly determine the number of cells
462 without removing the aggregates from the cell culture before inoculating a host.
463 Therefore, we analysed host-pathogen interaction using macrophages to elucidate how
464 the immune system might deal with *C. auris*. We observed that the uptake of single yeast
465 cells was not impeded in a noticeable way even if aggregates were present (Video V5).
466 Interestingly, macrophages interacted with aggregates but were unable to fully engulf or
467 clear them (Fig 9, Videos V1-V5). We also observed that many macrophages ignored
468 fungal cells which is in line with previous observations [41]. The inability of the immune
469 system to clear aggregates would explain their presence in animal models post infection
470 [18]. We hypothesize that cell aggregates might act as reservoirs in the host during
471 infection, with single cells being cleared by resident macrophages during active infection.
472 However, aggregates might persist for longer times, and cause breakthrough infections
473 when the immune system of the host is weakened or suppressed. Whether this explains
474 the higher virulence of an aggregative wild-type strain compared to a non-aggregative

475 *als4112* mutant requires further experimentation with primary human macrophages and
476 a whole-animal mammalian infection model.

477 To summarize, we have shown that there are two types of aggregation, canonical strain-
478 inherent aggregation induced by the growth environment, and a different morphology we
479 call “clustering” which is mediated by sub-inhibitory concentrations of echinocandins. We
480 have demonstrated that an ALS-family adhesin, Als4112, is involved in media-induced
481 aggregation, and that aggregates of both types pose a challenge for the immune system
482 and might be a cause of the persistence of *C. auris* systemic infections.

483

484 Materials & Methods

485 Yeast strains and culture conditions

486 All strains used in the study are listed in Table S6. All strains were recovered from storage
487 at -70 °C, grown for 1 day at 37 °C and maintained for up to 1 month on mycological YPD
488 (1% yeast extract (Oxoid Ltd., Basingstoke, UK), 2% mycological peptone (Oxoid Ltd.),
489 2% D-glucose (Thermo Fisher Scientific, Waltham, MA, USA) and 2% agar (Oxoid Ltd.))
490 slopes at 4 °C, with fresh cultures spread on mycological YPD plates and incubated at 37
491 °C for 2 days before use. All experiments were performed in Sabouraud dextrose
492 (SabDex) (1% mycological peptone (Oxoid Ltd.), 4% D-glucose (Thermo Fisher
493 Scientific)) or RPMI-1640 (10.4 g/L RPMI-1640 powder without phenol red (Merck KGaA,
494 Darmstadt, Germany), 1.8% D-Glucose (Thermo Fisher Scientific), 0.165 M 3-(N-
495 morpholino)propanesulfonic acid (Melford, Suffolk, UK) adjusted to pH 7 by 1 M NaOH
496 (Sigma-Aldrich, Burlington, MA, USA)). Cultures were grown at 37 °C shaking at 200 rpm.

497 Where plates have been used it is the medium specified with the addition of 2% agar
498 (Becton, Dickinson & Co., Franklin Lakes, NJ, USA).

499 The antifungal drugs, Caspofungin and Micafungin, were purchased from Merck KGaA
500 and resuspended in DMSO (Merck KGaA). For liquid culture they were added to RPMI-
501 1640 as prepared above at time of fungal inoculation. For agar plates, the antifungals
502 were added to RPMI-1640 with 2% agar after autoclaving and the media temperature had
503 cooled to 60 °C to avoid degradation of the antifungal activity.

504 **Determination of Aggregation**

505 Strains were grown for 16 hours at 37 °C shaking at 200 rpm. Cells were harvested by
506 centrifugation (2,500 ×*g*, 5 minutes) after which culture media was removed. Cells where
507 then resuspended in 1× phosphate buffer saline (1× PBS) or ddH_2O this was repeated
508 twice to completely remove growth media. Cells finally suspended in 1× PBS or ddH_2O
509 were vortexed for 1 minute before microscopic examination to check for presence of
510 aggregates.

511 **Microscopy**

512 For light microscopy cells were suspended in the indicated solution and 50 µL was added
513 to a glass slide before images were captured on a Zeiss Axioskop 20 microscope with a
514 Axiocam 105 Colour using Zen 2.3 software (version 2.3.69.10000).

515 For fluorescence microscopy, cells were fixed with 4% methanol-free paraformaldehyde
516 overnight, cells were harvested by centrifugation (2,000 ×*g*, 5 minutes) and resuspended
517 in 1× PBS, this was repeated twice to remove traces of paraformaldehyde.

518 For cell wall chitin, cells were incubated for 1 hour with 10 µg/mL Calcofluor White M2R
519 (CFW) (Merck KGaA). Cells were harvested by centrifugation (2,000 ×*g*, 5 min) and
520 supernatant removed. Cells were resuspended in 10 µL Vectashield HardSet Antifade
521 Mounting Medium (2B Scientific, Kidlington, UK), which was placed on a microscope
522 glass slide and coverslip placed on top without applying pressure. Images were captured
523 on a Zeiss Imager M2 upright microscope with a Hamamatsu Flash 4 LT camera using
524 Zen 2.3 software (version 2.3.69.1018).

525 For confocal fluorescent microscopy of chitin and mannan staining, fixed cells were
526 incubated with 1× PBS containing 1% bovine serum albumin (Merck KGaA) for 1 hour on
527 ice. This was removed by centrifugation (2,000 ×*g*, 5 min) and cells were resuspended in
528 1× PBS containing 10 µg/mL CFW and 25 mg/mL Concanavalin A (Con A) conjugated to
529 Alexa Fluor 488 for 1 hour on ice. Cells were harvested by centrifugation (2,000 ×*g*, 5
530 min) and resuspended in 1× PBS, this was repeated twice. After the final wash with 1×
531 PBS, cells were spun down again and supernatant was removed, cells were then re-
532 suspended in 10 µL Vectashield HardSet Antifade Mounting Medium and mounted onto
533 microscope slides, a coverslip was applied without pressure. Images were taken as Z-
534 stacks with an image every 0.1 µm with a Ultraview VoX spinning disk confocal
535 microscope using a Hamamatsu C11440-22C camera. Images were processed with
536 Volocity software (Version 6.5.1) selecting images that showed the connection point
537 between cells.

538 ***Galleria mellonella* survival assay**

539 Strains were prepared for inoculation by picking a single colony from a SabDex plate and
540 growing the cells for 16 hours in fresh liquid medium (SabDex or RPMI-1640). Medium

541 was removed by centrifugation (2,500 ×*g*, 5 minutes). Cells where then washed twice with
542 ddH_2O by centrifugation (2,500 ×*g*, 5 minutes) between each resuspension. Finally, cells
543 were suspended in 1× PBS. Cell suspensions stood for 10 minutes to allow aggregates
544 to sink to the bottom of the suspension and single cells were harvested from the top layer
545 of the solution for counting. Cells were adjusted to give a final inoculum of 50 µL
546 containing 5×10^5 cells in 1× PBS. *G. mellonella* larvae (TruLarv BioSystems
547 Technology, Exeter, UK or UK Waxworms Ltd, Sheffield, UK) were inoculated within two
548 days of receipt. A 50 µL inoculum was given via the last left proleg with a 0.5 ml 29G
549 Micro-Fine U-100 insulin injection unit (BD Medical, Franklin Lakes, NJ, USA).

550 Larvae were incubated for 6 days at 37 °C. Every 24 hours larvae were examined and
551 deemed dead when they no longer responded to physical stimuli. Each experiment also
552 had a non-injected control group and a control group injected with 1× PBS only. Results
553 were pooled across three independent experiments and statistical analysis was done
554 using a Kaplan-Meier survival plot followed by Log-rank test statistics to determine if
555 differences in survival were significant.

556 **MIC Testing**

557 Minimum inhibitory concentration (MIC) determination was done using Caspofungin and
558 Micafungin MIC E-test strips (Liofilchem srl, Roseto degli Abruzzi, Italy) following the
559 manufacturer's guidance with small modifications. Isolates were grown for 24 hours on
560 SabDex agar plates, one colony was picked and dispersed in ddH_2O. Onto RPMI-1640
561 agar plates 2×10^6 cells were spread and allowed to dry for 10 minutes. A MIC test strip
562 was carefully placed onto the agar surface, and the plate was incubated for 24 hours at
563 37 ˚C before determining the zone of inhibition and the MIC or MIC_{90} where appropriate.

564 **High-pressure freezing sample preparation for transmission electron microscopy**
565 **(TEM)**

566 Cells were grown for 16 hours in the indicated media. Cells were then harvested by
567 centrifugation (2,500 ×*g*, 5 minutes) and removal of excess cell culture media was
568 performed before fixation and preparation. Fixation and preparation were performed by
569 the Microscopy and Histology Core Facility at the University of Aberdeen following a
570 published protocol [42]. Fixation was done by high-pressure freezing using a Leica
571 Empact 2/RTS high-pressure freezer. Samples were returned to us and we performed
572 imaging using a JEOL 1400 plus transmission electron microscope with an AMT UltraVUE
573 camera. All images were processed, and cell wall thickness was measured with Fiji
574 (ImageJ version 1.53f51) [43].

575 **Proteinase K assay**

576 Cells were grown for 16 hours in the indicated liquid medium at 37 ˚C shaking at 200 rpm.
577 Cells were harvested by centrifugation (2,500 ×*g*, 5 minutes), the supernatant was
578 discarded before the pellet was resuspended in 1× PBS, centrifugation and resuspension
579 was repeated twice before aggregates were counted using a haemocytometer. For the
580 assay 1×10^6 cells were added to 50 µL of ddH_2O either containing 12.5 µg of proteinase
581 K or not before being incubated for 1 hour at 50 ˚C, a second ddH_2O sample was also
582 prepared and incubated at room temperature for 1 hour to ensure the application of heat
583 did not increase the number of aggregates. After incubation 950 µL 1× PBS was added,
584 and cells were vortexed at high speed for 1 minute. The number of aggregates were
585 counted again with a haemocytometer and the fold-change of aggregates between the

586 unincubated against the incubated samples calculated. Statistical significance was
587 determined by an independent samples t-test.

588 **Transcriptomics**

589 UACa20 (clade III) and UACa11 (clade I) were grown in the specified media for 16 hours
590 and RNA was extracted for RNA-sequencing (RNA-seq) using the method outlined below,
591 this was repeated three times on independent colonies at different times. After growth for
592 16 hours cells were harvested by centrifugation (2,500 ×*g*, 5 minutes). Supernatant was
593 discarded and cells resuspended in residual supernatant before immediately proceeding
594 to RNA extraction. RNA was extracted by homogenisation of cells with acid-washed glass
595 beads in 600 µL TRIazole (Invitrogen, Thermo Fisher Scientific, Waltham, MA, USA) per
596 60 µL culture using a FastPrep-24 5G (MP Biomedicals, Santa Ana, CA, USA) for cell
597 lysis. Glass beads and cell debris were discarded after centrifugation (12,000 ×*g* for 10
598 minutes at 4 °C) and the supernatant was used for further steps. Addition of 0.2 mL
599 chloroform per 1 mL TRIazole was followed by vigorous shaking for 15 seconds and
600 incubation at room temperature for 2 minutes. Centrifugation (12,000 ×*g* for 15 minutes
601 at 4°C) separated the proteins, DNA, and RNA into 3 phases. RNA in the aqueous layer
602 was removed and subjected to precipitation by addition of 500 µL isopropanol and
603 incubated at room temperature for 10 minutes. Centrifugation (12,000 ×*g* for 10 minutes
604 at 4°C) resulted in a pellet of RNA, which was washed with 600 µL 75% ethanol. Ethanol
605 was removed after centrifugation (6,000 ×*g* for 10 minutes at 4°C) and the RNA pellet
606 was dried for 10 minutes at room temperature. The RNA samples were resuspended in
607 RNase-free water before clean-up treatment with the RNase-Free DNase Set (Qiagen,
608 Hilden, Germany) following the manufacturer's protocol for off-column clean-up. RNA was

609 then subjected to further clean-up by using the RNeasy Mini Kit (Qiagen) following the
610 manufacturer's instructions, before final suspension in RNase-free water and storage at
611 -80 °C before sequencing.

612 Sequencing of mRNA was carried out by the Centre for Genome-Enabled Biology and
613 Medicine (CGEBM) at the University of Aberdeen. Before sequencing External RNA
614 Controls Consortium (ERCC) spike controls were added to samples for assessment of
615 library quality and as estimation of lowest limit of detection [44]. Library preparation was
616 done using Illumina TruSeq Stranded mRNA kit (Illumina Inc., San Diego, CA, USA) and
617 sequenced using the High Output 1×75 kit on the Illumina NextSeq 500 platform
618 producing 75 bp single-end reads. Quality control of the sequencing data was performed
619 using FastQC (version 0.11.8)
620 (https://www.bioinformatics.babraham.ac.uk/projects/fastqc/) with lower-quality reads
621 and adaptor content being removed with TrimGalore! (version 0.6.4)
622 (http://www.bioinformatics.babraham.ac.uk/projects/trim_galore/) with a Phred quality
623 score threshold of 30. ERCC spike controls consist of 92 synthesized transcripts that
624 range both in length and concentration. Two mixes (Mix 1 and Mix 2) are provided with
625 differing transcript concentration ratios of 4:1, 1:1, 1:1.5, and 2:1 to allow for assessment
626 of detection of differential expression. One of these two mixes was randomly added to
627 each of the samples. ERCC reads were removed by aligning all reads to the ERCC
628 reference genome using HISAT2 (version 2.1.0) [45] with unmapped *C. auris* reads being
629 kept for alignment. Illumina-sequencing produced between ~25 million and ~30 million
630 reads per sample (Table S7).

631 The *C. auris* B11221 reference genome was downloaded from NCBI
632 (https://www.ncbi.nlm.nih.gov/genome/38761?genome_assembly_id=678645) [46]
633 along with the equivalent annotation file and prepared for use with the alignment software
634 HISAT2 (version 2.1.0) [45]. Reads were aligned to this prepared reference using HISAT2
635 (version 2.1.0) [45] with the parameter for stranded library preparation used. SAMtools
636 (version 1.9) [47] was used to process the alignments and reads were counted at gene
637 locations using featureCounts (part of the sub-read version 1.6.2 package) [48] utilizing
638 the parameter to split multi-mapped reads as a fraction across all genes that they align
639 to, and the parameter for stranded analysis. 83.66% to 88.75% of reads aligned to coding
640 regions and after quality control and removal of low-count genes a total of 5,431 genes
641 remained for analysis.

642 edgeR (version 3.30.3) [49] was used to detect which genes had a significant differential
643 change in expression. All genes that had a CPM (count per million) value of more than
644 one in three or more samples were kept for analysis, and all other genes were removed
645 as low-count genes. Differential expression analysis was performed via pairwise
646 comparisons between each sample group. To obtain the B8441 gene names, the gene
647 DNA sequence for the B11221 strain was obtained and compared to the B8441 gene
648 sequences using BlastN [50].

649 ***als4112* mutant generation**

650 All genomic DNA was prepared as described previously [12]. All PCRs were done using
651 VeriFi Hot Start Mix (PCR Biosystems Ltd., London, UK), with the exception of
652 transformant screening which was done with PCRBIO Taq Mix Red (PCR Biosystems
653 Ltd.). The deletion mutant was generated by a previously described method of homology-

654 directed repair and lithium-acetate transformation [51] using a nourseothricin marker.
655 Briefly, the *CaNAT1* resistance marker was amplified from plasmid pALo218 using
656 primers oUA315 and oUA316 (Table S8) [12]. The *ALS4112* gene sequence and flanking
657 sequences 2 kb upstream and downstream were obtained from NCBI (Accession
658 XP_028889036.1) to design primers, 1 kb upstream and 1 kb downstream of *ALS4112*
659 was amplified with primers oUA989 and oUA990, and oUA991 and oUA992 respectively,
660 from UACa20 genomic DNA (Table S8). The deletion cassette was assembled using
661 fusion PCR and primers oUA993 and oUA994 (Table S8) to amplify the final deletion
662 cassette which was confirmed by gel electrophoresis. UACa20 (clade III) was grown
663 overnight at 30 ºC with shaking before being diluted 1:100 in fresh bacteriological YPD
664 (1% yeast extract (Oxoid Ltd.), 2% bacteriological peptone (Oxoid Ltd.), 2% D-glucose
665 (Thermo Fisher Scientific) and 2% agar (Oxoid Ltd.)) and grown for a further 4 hours.
666 Cells were then harvested by centrifugation for 2 minutes at 1,000 ×*g* and resuspended
667 in ddH_2O. This step was repeated twice before cells were suspended in 0.1 M lithium
668 acetate and were centrifuged again for 1 minute at 1,000 ×*g* before being suspended in
669 0.1 M lithium acetate. To this 5 µg of the deletion cassette in 50 µL of 50% PEG-3350, 1
670 M lithium acetate and 10 mg/mL denatured herring sperm DNA (Thermo Fisher Scientific)
671 was added and incubated overnight shaking at 30 ºC. Heat shock was applied in a heat
672 block the next day at 44 ºC for 15 minutes, and cells were resuspended in bacteriological
673 YPD and incubated shaking at 30 ºC for 3 hours to recover. After recovery cells were
674 plated on bacteriological YPD plates containing 200 µg/mL nourseothricin (clonNAT;
675 Werner BioAgents GmbH, Jena, Germany) and incubated at 30 ºC until colonies
676 appeared (usually 2 days). Transformants were screened for *als4112* deletion with

677 primers oUA987 and oUA988 (Table S8), and UACa20 genomic DNA was used as a
678 positive control.

679 **Inverse PCR**

680 Genomic DNA from the *als4112* null mutant was prepared as described previously [12].
681 Inverse PCR design is outlined in Fig S4. For the restriction digest 1 µg of genomic DNA
682 from UACa20 and *als4112*Δ was incubated for 1 hour at 37 ºC with the restriction
683 endonuclease BamHI-HF (New England Biolabs (NEB), Ipswich, MA, USA) following the
684 manufacturer's instructions. The enzyme was removed with the Monarch PCR & DNA
685 Cleanup Kit (NEB) following the manufacturer's instructions. For the ligation reaction 8 µL
686 of the digest was treated with T4 Ligase (NEB) for 16 hours at 16 ºC, before stopping the
687 reaction at 65 ºC for 10 minutes. PCR was done using VeriFi Hot Start Mix (PCR
688 Biosystems Ltd.) to amplify DNA for sequencing with primers oUA995 and oUA996 (Table
689 S8) for upstream region boundary of the deletion cassette and primers oUA997 and
690 oUA998 (Table S8) were used for the downstream boundary of the deletion cassette,
691 amplification of the *als4112*Δ DNA but not UACa20 DNA was confirmed by gel
692 electrophoresis. DNA was sent for Sanger sequencing (Eurofins Scientific, Luxembourg,
693 Luxembourg) with primers oUA999 for upstream and oUA1000 for downstream
694 sequencing (Table S8), and results were compared using BLAST against the *C. auris*
695 reference genome (NCBI Cand_auris_B11221_V1) to determine boundaries of the
696 deletion cassette.

697 **THP-1 Macrophage Differentiation**

698 The human monocyte cell line THP-1 (MerckKGaA) were maintained at 2×10^5 cells/mL
699 in RPMI-1640 containing 10% fetal bovine serum (FBS) (Thermo Fisher Scientific), 200

700 U/mL penicillin/streptomycin (Thermo Fisher Scientific), and 2 mM GlutaMAX (Thermo
701 Fisher Scientific) at 37 °C in 5% CO_2. Macrophages were differentiated with 200 nM
702 phorbol 12-myristate 13-acetate (PMA) (Merck KGaA) following a previously described
703 method with slight modifications [52]. Briefly 1 × 10^5 cells/ml were incubated in RPMI-
704 1640 with 200 nM PMA, 10% FBS, 200 U/mL penicillin/streptomycin, and 2 mM
705 GlutaMAX at 37 °C in 5% CO_2 for 3 days. PMA-containing media and non-adherent cells
706 were removed by washing twice with 1× PBS. THP-1 macrophages were then allowed to
707 rest for 3 days in RPMI-1640 with 10% FBS, 200 U/mL penicillin/streptomycin, and 2 mM
708 GlutaMAX at 37 °C in 5% CO_2. Media was removed and THP-1 macrophages were lifted
709 by scraping. 2 × 10^5 THP-1 macrophages were added to each well of an 18-well slide
710 (ibidi, Gräfelfing, Germany) in RPMI-1640 supplemented with 10% FBS, 200 U/mL
711 penicillin/streptomycin, and 2 mM GlutaMAX at 37 °C in 5% CO_2 and allowed to rest for
712 a further 24 hours before being used for experimentation.

713 **Live-Cell Imaging**

714 Fungal cells were grown for 24 hours in desired media and cells were harvested by
715 centrifugation 2,000 ×*g* for 5 minutes and resuspended in ddH_2O, this was repeated twice
716 before cells were counted with a haemocytometer. Medium was removed from THP-1
717 macrophages and replaced with CO_2-independent medium (Fisher Scientific) containing
718 fungal cells at MOI 1:3 and 0.02 µg/µL propidium iodide (Fisher Scientific). Images were
719 taken every 3 min for 2 hours on an Ultraview VoX spinning disk confocal microscope
720 using Volocity software (Version 6.5.1).

721 **Statistics**

722 All statistics were performed in SPSS Statistics for Windows (version 28.0) (IBM Corp.,
723 Armonk, NY, USA) except for log-rank tests of *G. mellonella* survival data which were
724 performed in R (version Rx64, 4.3.0) (http://www.r-project.org/).

725

726 **Acknowledgments**

727 We are grateful to Rhys Farrer (MRC CMM, University of Exeter) for guidance on
728 bioinformatic analysis, to Louise Walker (University of Aberdeen) for advice on
729 macrophage work, and to Neil A. R. Gow (MRC CMM, University of Exeter) and Dhara
730 Malavia (MRC CMM, University of Exeter) for discussing their unpublished results. We
731 thank Gillian Milne (Microscopy & Histology Facility, University of Aberdeen) for technical
732 assistance with electron microscopy. *Candida auris* strains were kindly provided by
733 Anuradha Chowdhary (Vallabhbhai Patel Chest Institute, University of Delhi, Delhi, India),
734 Public Health England (PHE) (Bristol, UK), and the Mycotic Diseases Branch of the
735 Centers for Disease Control and Prevention (CDC) (Atlanta, GA, USA).

736

737 **Funding**

738 This work was supported by a PhD studentship (MR/P501955/1) from the Medical
739 Research Council (MRC) Centre for Medical Mycology at the University of Exeter, UK
740 (MR/N006364/2). The funders had no role in study design, data collection and analysis,
741 decision to publish, or preparation of the manuscript.

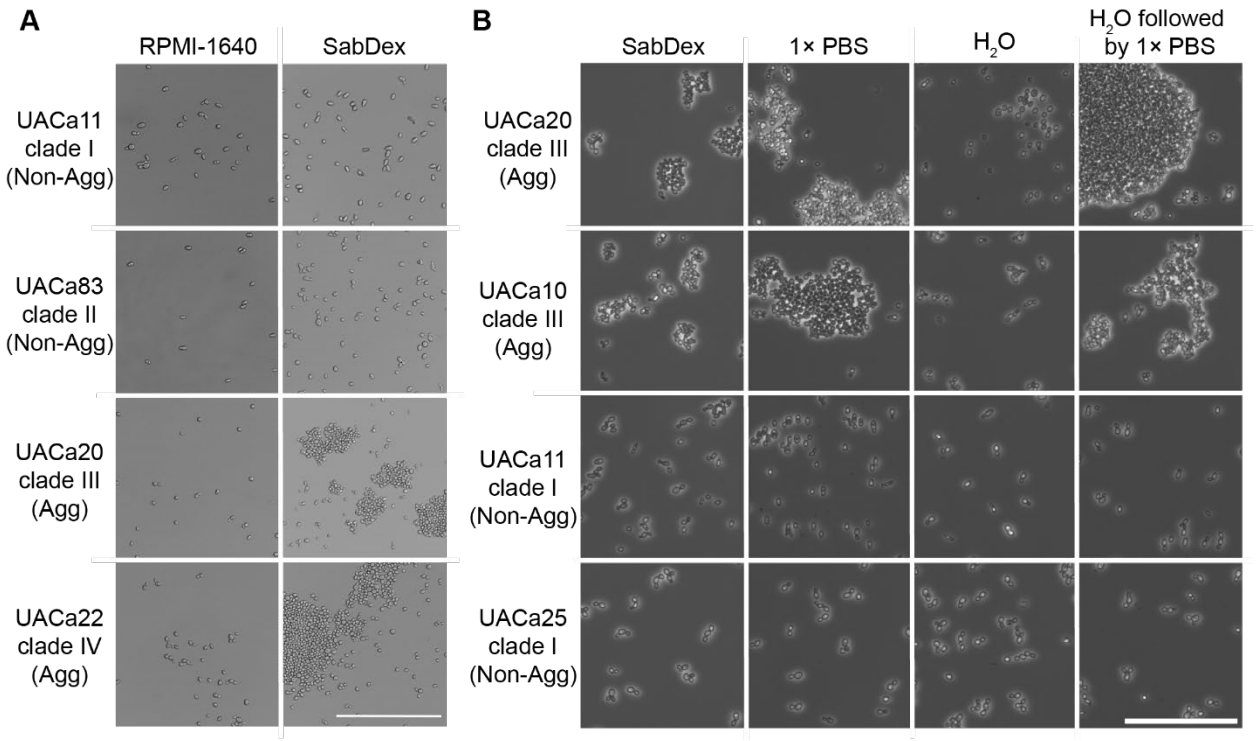

Fig 1. Aggregation is an inducible phenotype. (**A**) Changes in growth media induce aggregation only in aggregative strains. Light microscopic (brightfield) images of cells of the indicated strains (left) in the indicated medium (top). Cells grown in RPMI-1640 displayed no aggregation regardless of ability to aggregate. Only aggregative (Agg) strains grew as aggregates when grown in SabDex while non-aggregative (Non-Agg) strains remained as single cells. (**B**) Aggregation is lost when media is replaced with water but is retained when replaced with 1× PBS. Light microscopy (phase contrast) of cells grown overnight in SabDex followed by either replacement of media with ddH_2O, 1× PBS, or ddH_2O followed by 1× PBS. Non-aggregative (Non-Agg) strains were unaffected by the suspension liquid while aggregative (Agg) strains retained aggregation when suspended in 1× PBS, but aggregates were noticeably reduced after washing with ddH_2O. Scale bars represent 50 μm.

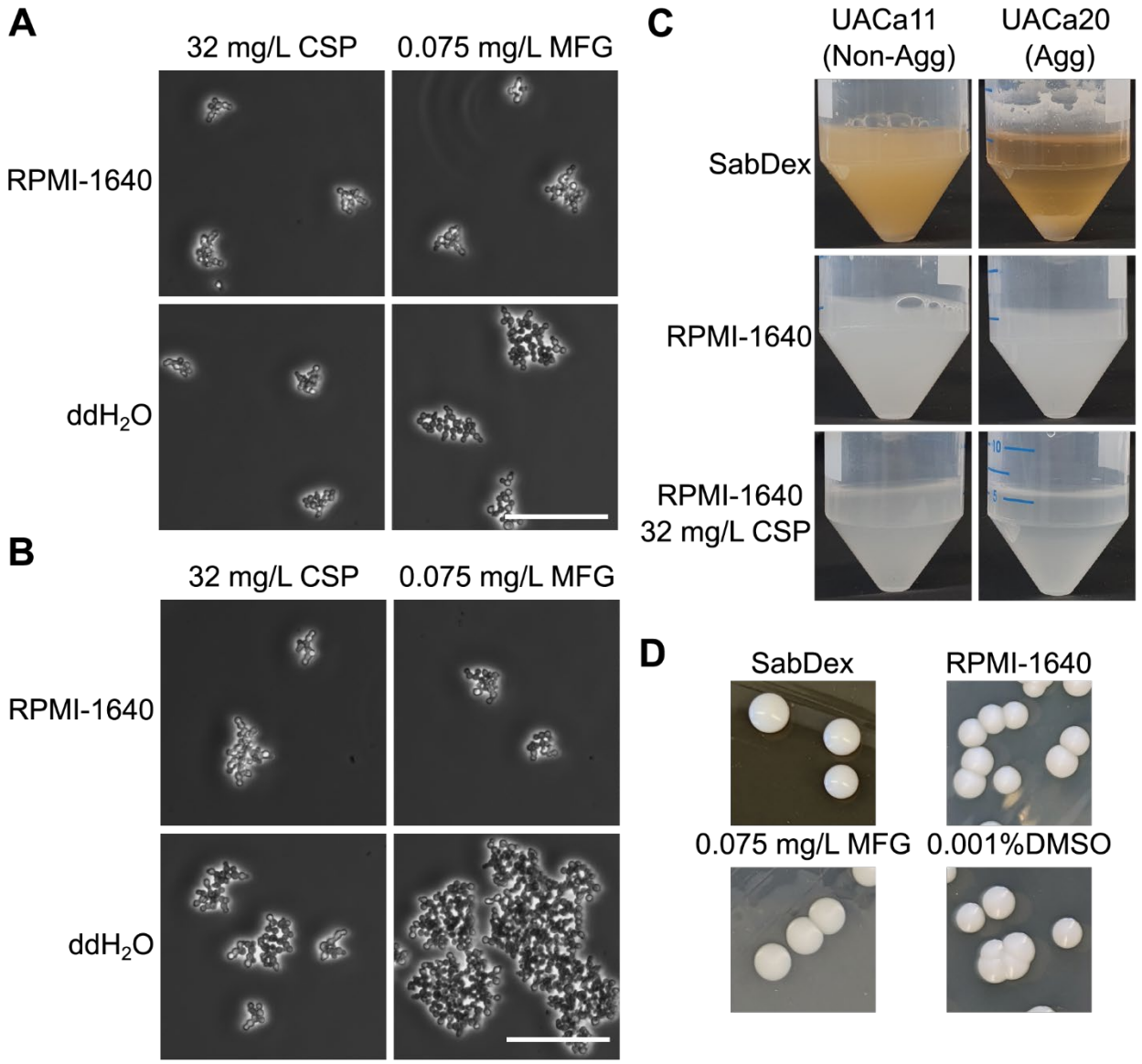

754
755 **Fig 2. Sub-inhibitory concentrations of echinocandins induce a different type of**
756 **aggregation (clustering).** (**A**) UACa20 (clade III) and (**B**) UACa11 (clade I) grown overnight in
757 RPMI-1640 containing either 32 mg/L CSP or 0.075 mg/L MFG, images were taken with a light
758 microscope (phase contrast) of cells in media and when resuspended in ddH_2O, showing drug-
759 induced clusters remain intact after washing with ddH_2O. Scale bars in (A) and (B) represent 50
760 µm. (**C**) Differences in sedimentation were not observed in the RPMI-1640 cultures or the drug-
761 induced clusters, while media-induced aggregates did fall out of suspension. (**D**) Colony
762 morphology was not conspicuously impacted by aggregation.

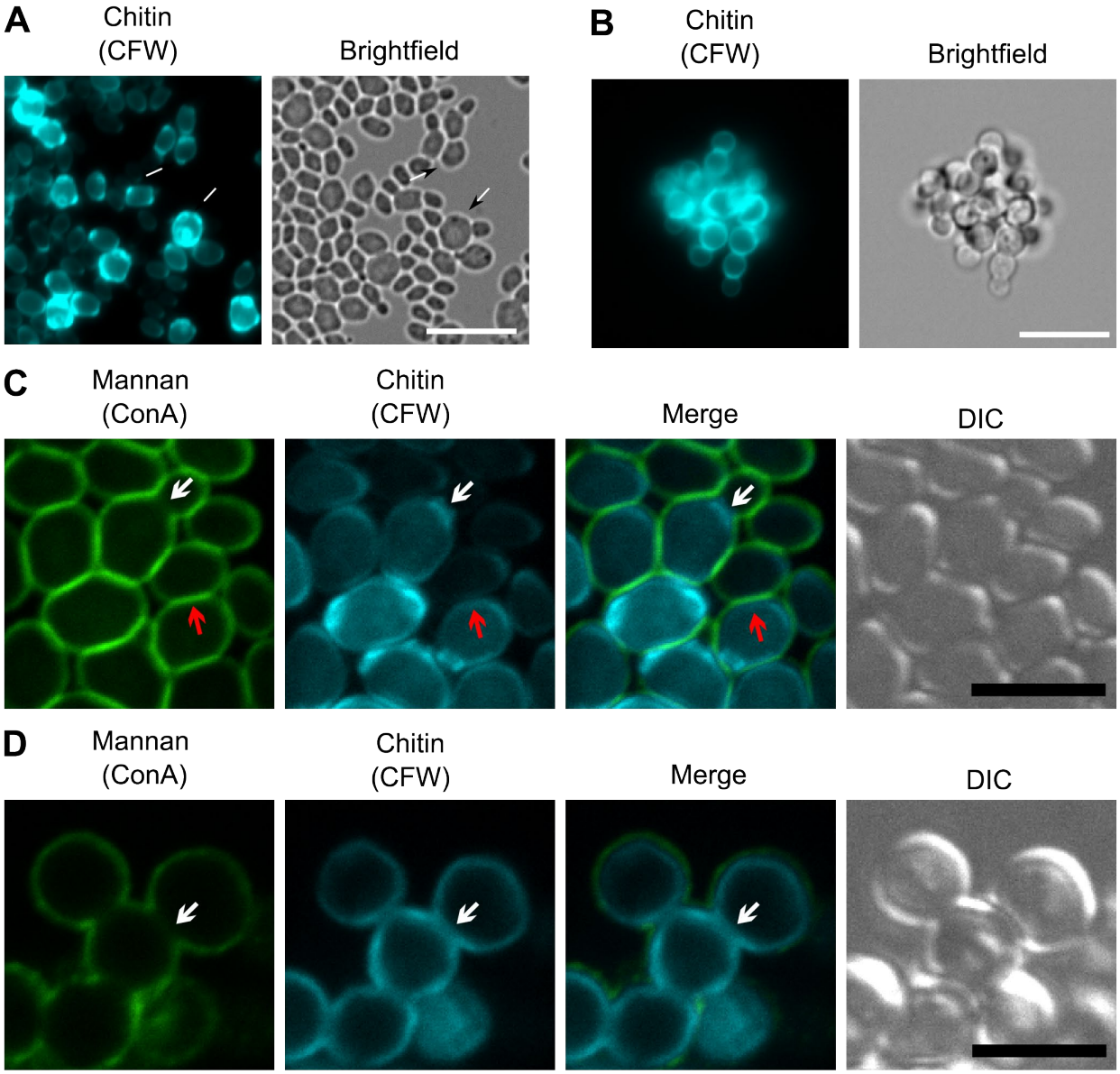

Fig 3. Differences in chitin bud scars and the coverage of outer cell wall mannan indicate differences between aggregation types. (**A, B**) UACa20 (clade III) cells grown overnight in SabDex (A) or RPMI-1640 containing 32 mg/L CSP (B), cell wall chitin is visualized with 10 µg/mL CFW. White arrows point to bud scars without daughter cells grown in SabDex indicating full cell separation after division, this is not seen on antifungal-induced aggregation. Scale bars in (A) and (B) represents 10 µm. (**C, D**) Cell wall mannan and chitin stained with ConA and CFW, respectively, visualized by confocal microscopy to generate image sections of entire aggregates. (**C**) Cells grown in SabDex are completely outlined by mannan and chitin staining (red arrows), even where cells are closely juxtaposed, only actively dividing cells with small daughter buds appear to have a break in the mannan outer cell wall layer (white arrows). (**D**) When grown in RPMI-1640 containing 0.075 mg/L MFG cells are completely bounded by chitin, but display a lack of mannan staining at cell-cell junctions (white arrows) indicating a cell separation defect. In (C) and (D) the scale bars represent 5 µm.

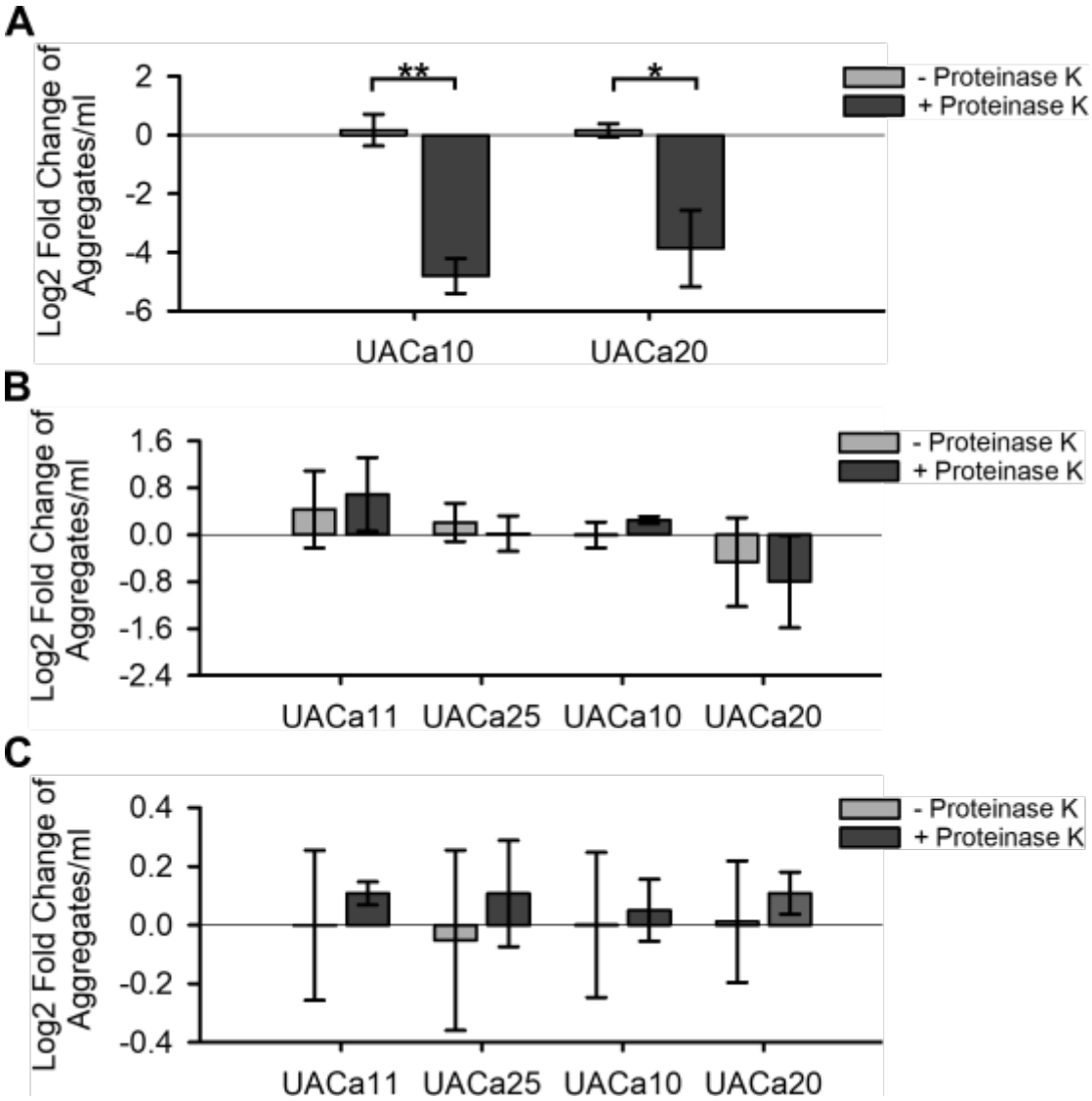

Fig 4. Proteinase K treatment significantly reduces media-induced aggregation but not antifungal-induced clustering. Log_2-fold change in aggregate/cluster numbers grown in SabDex (**A**), 32 mg/L CSP (**B**), or 0.075 mg/L MFG (**C**) after incubation at 50 °C for 1 hour with or without 12.5 µg of proteinase K. *$p < 0.05$, **$p < 0.001$, as determined by independent samples t-test.

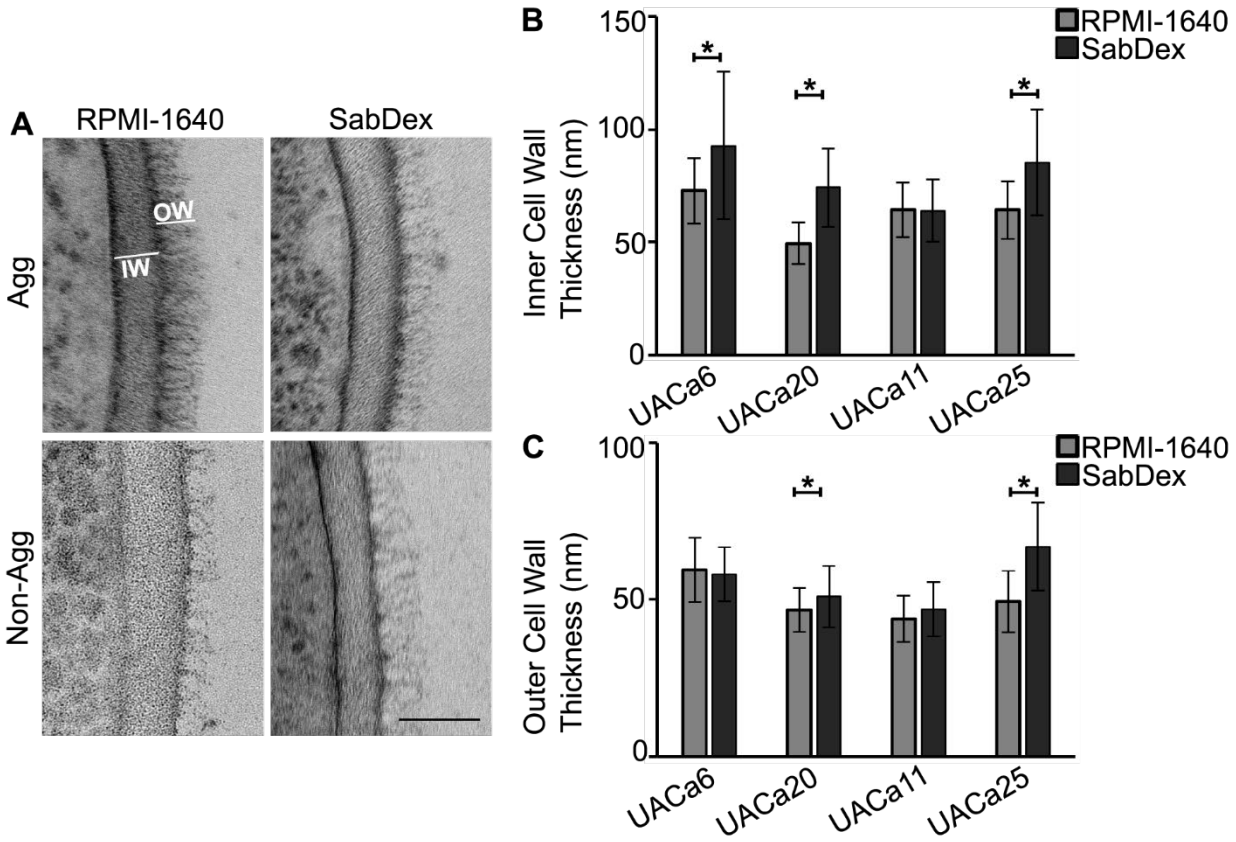

Fig 5. Media-induced aggregation does not cause changes to the cell wall ultrastructure. Cells grown in indicated media were fixed by high pressure freezing for transmission electron microscopy TEM. (**A**) Representative images from TEM of cell wall of an aggregative (Agg) and a non-aggregative (Non-Agg) strain, outer cell wall (OW) and inner cell wall (IW) are indicated. Scale bar represents 50 nm. (**B**) Inner cell wall measurements show strain-specific changes in response to culture conditions. (**C**) Length of mannan fibrils (outer cell wall) shows moderate changes in response to culture conditions in two isolates, UACa20 (clade III) (Agg) and UACa25 (clade I) (Non-Agg). *$p < 0.05$ as determined by independent samples t-test.

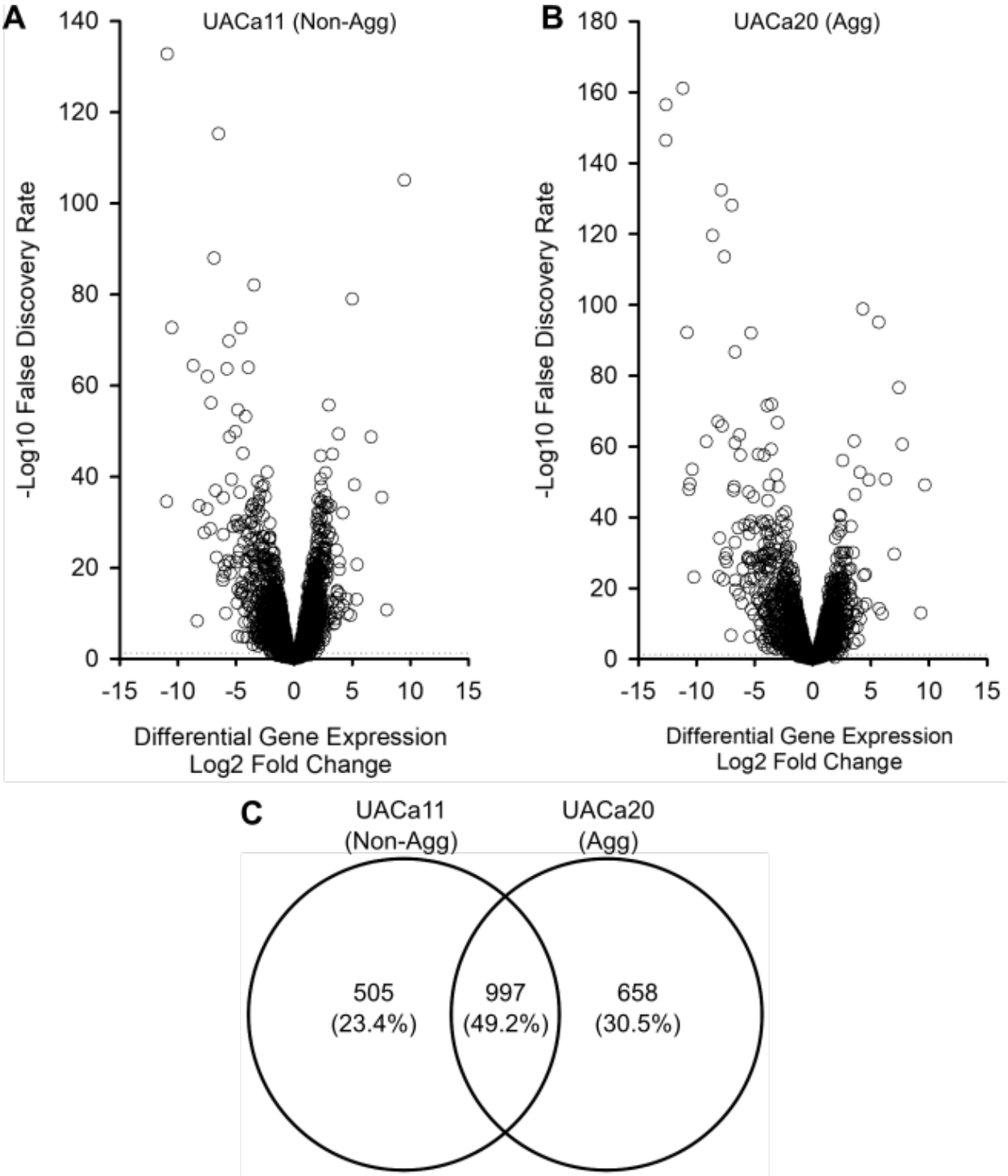

Fig 6. Differential expression of genes (DEGs) in an aggregative and a non-aggregative strain grown in SabDex or RPMI-1640. Aggregative (Agg) clade III strain UACa20 and non-aggregative (Non-Agg) clade I strain UACa11 were grown in the specified media for 16 hours and RNA was extracted for RNA-seq, this was repeated three times on independent colonies at different times. (**A, B**) Volcano plots of the total DEGs for UACa11 (A) and UACa20 (B) are shown with the dotted line indicating an FDR = 0.05. (**C**) Venn diagram of statistically significant (FDR < 0.05) DEGs, numbers indicate how many DEGs are unique to UACa11 and UACa20 and what portion of DEGs are shared between the strains.

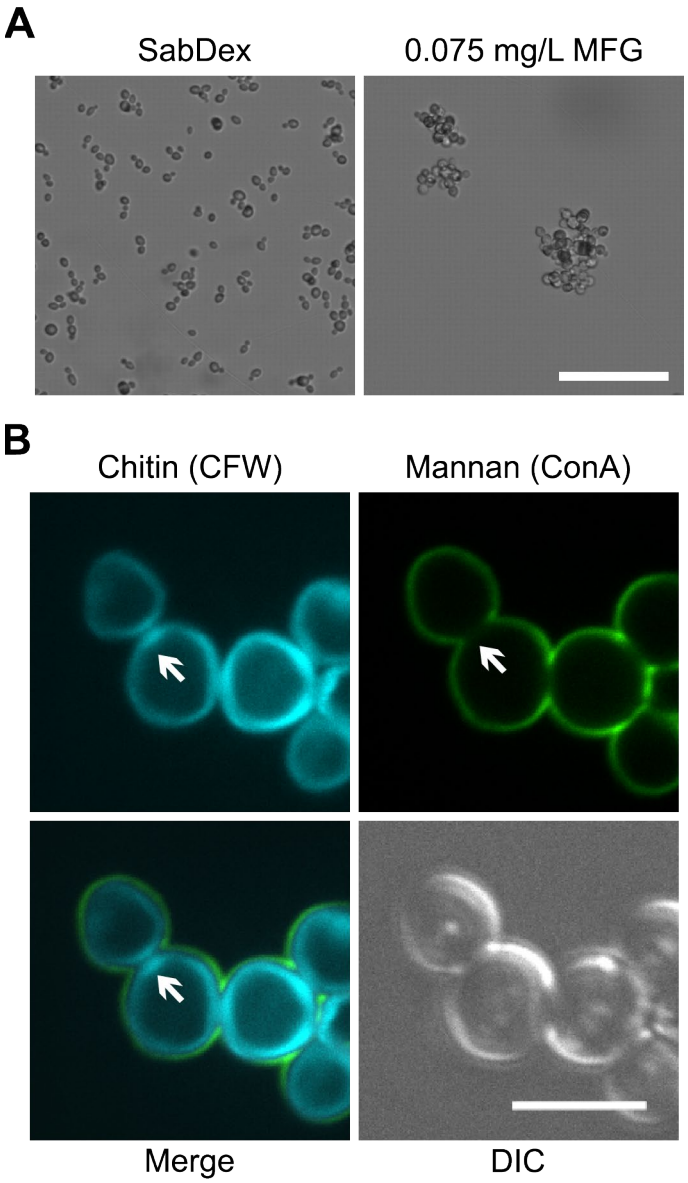

Fig 7. *ALS4112* seems to be required for media-induced aggregation, but not for antifungal-induced clustering. (**A**) Light microscopy images (contrast) of the *als4112*Δ mutant grown SabDex or RPMI-1640 containing 0.075 mg/L MFG for 24 hours. Cells grown in SabDex failed to aggregate, whereas cells grown in the presence of MFG did form clusters. Scale bar represent 10 μm. (**B**) The *als4112*Δ mutant was grown for 24 hours in RPMI-1640 containing 0.075 mg/L MFG and was imaged by confocal microscopy. Total cell wall chitin was stained with CFW and mannans stained with ConA. White arrows highlight features consistent with antifungal-induced clustering, where cells are completely surrounded by chitin staining, but display a lack of mannan staining at cell-cell junctions. Scale bar represents 5 μm.

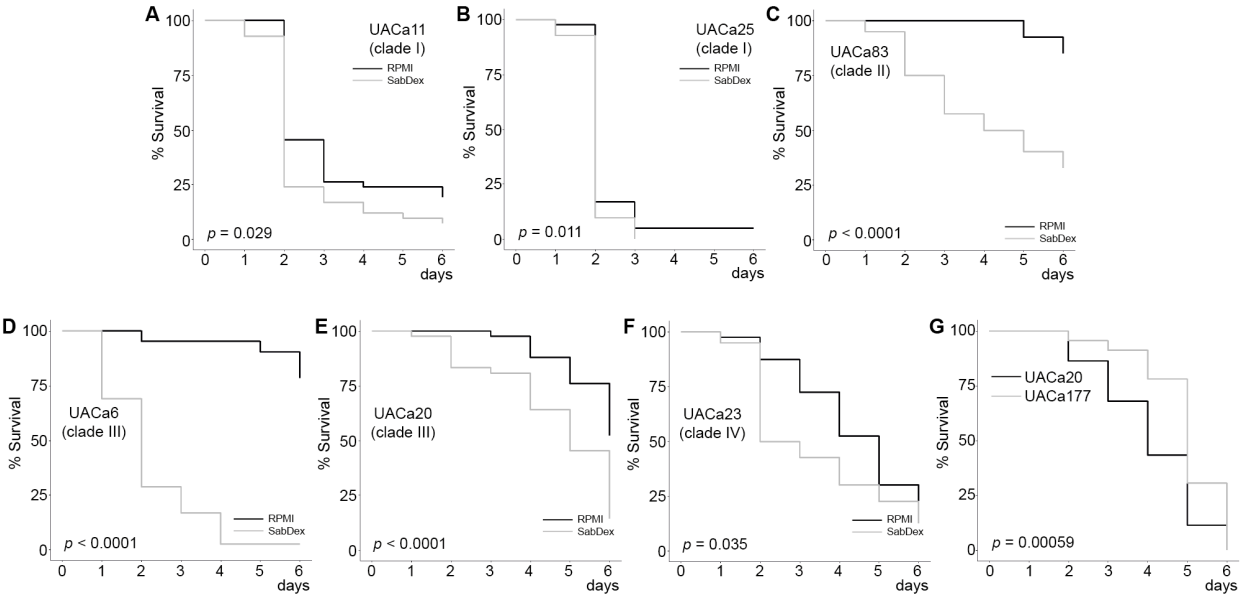

Fig 8. Virulence in the *G. mellonella* infection model is dependent on pre-growth media and Als4112. (**A-C**) Non-aggregative and (**D-F**) aggregative *C. auris* strains were grown in RPMI-1640 or SabDex before inoculation into *G. mellonella* larvae. All strains except UACa25 (clade I) in (B) showed significant differences in virulence dependent on the media used to grow the fungal cells before inoculation. (**G**) Wild-type (UACa20) and *als4112*Δ (UACa177) *C. auris* cells were grown in SabDex before inoculation into *G. mellonella* larvae (A log-rank test was used to calculate *p*-values . 30 larvae in 3 independent experiments were used to assess virulence.

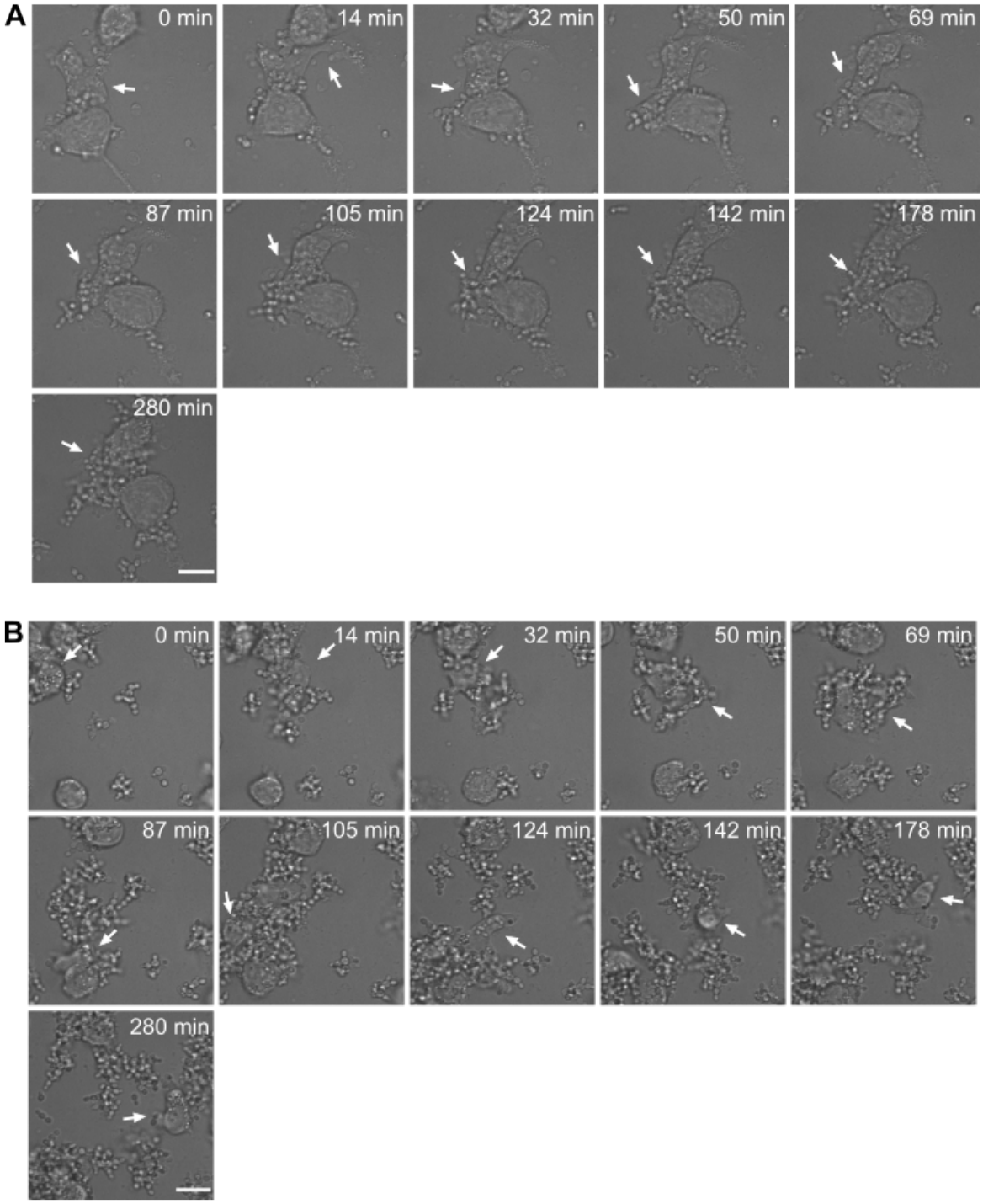

Fig 9. Macrophages have difficulty in clearing large aggregates and clusters. (**A**) Aggregates of strain UACa20 (clade III) grown in SabDex were co-incubated with THP-1 derived macrophages, and one macrophage was followed for the duration of the experiment (white arrow), taken from Video V3. (**B**) Clusters of strain UACa20 grown in RPMI-1640 containing 0.075 mg/L MFG, one macrophage was followed for the duration of the experiment (white arrow), taken from Video V4. Scale bars represent 15 μm.

827 **References**

828 1. Satoh K, Makimura K, Hasumi Y, Nishiyama Y, Uchida K, Yamaguchi H. *Candida auris* sp.
829 nov., a novel ascomycetous yeast isolated from the external ear canal of an inpatient in a
830 Japanese hospital. Microbiol Immunol. 2009;53: 41–44. doi:10.1111/j.1348-
831 0421.2008.00083.x

832 2. Rhodes J, Fisher MC. Global epidemiology of emerging *Candida auris*. Curr Opin
833 Microbiol. 2019;52: 84–89. doi:10.1016/j.mib.2019.05.008

834 3. Forsberg K, Woodworth K, Walters M, Berkow EL, Jackson B, Chiller T, et al. *Candida*
835 *auris*: The recent emergence of a multidrug-resistant fungal pathogen. Med Mycol.
836 2019;57: 1–12. doi:10.1093/mmy/myy054

837 4. Stephenson JC, Garza DR, Bouklas T. A fungus for our time: *Candida auris* emerges into
838 the anthropocene. Curr Trop Med Rep. 2023. doi:10.1007/s40475-023-00293-w

839 5. Lockhart SR, Etienne KA, Vallabhaneni S, Farooqi J, Chowdhary A, Govender NP, et al.
840 Simultaneous emergence of multidrug-resistant *Candida auris* on 3 continents confirmed
841 by whole-genome sequencing and epidemiological analyses. Clinical Infectious Diseases.
842 2017;64: 134–140. doi:10.1093/cid/ciw691

843 6. Chow NA, de Groot T, Badali H, Abastabar M, Chiller TM, Meis JF. Potential fifth clade of
844 *Candida auris*, Iran, 2018. Emerg Infect Dis. 2019;25: 1780–1781.
845 doi:10.3201/eid2509.190686

846 7. Arastehfar A, Shaban T, Zarrinfar H, Roudbary M, Ghazanfari M, Hedayati M-T, et al.
847 Candidemia among Iranian patients with severe COVID-19 admitted to ICUs. Journal of
848 Fungi. 2021;7: 280. doi:10.3390/jof7040280

849 8. Noble SM, Gianetti BA, Witchley JN. *Candida albicans* cell-type switching and functional
850 plasticity in the mammalian host. Nat Rev Microbiol. 2017;15: 96–108.
851 doi:10.1038/nrmicro.2016.157

852 9. Iracane E, Vega-Estévez S, Buscaino A. On and Off: epigenetic regulation of *C. albicans*
853 morphological switches. Pathogens. 2021;10: 1463. doi:10.3390/pathogens10111463

854 10. Kumamoto CA, Vinces MD. Contributions of hyphae and hypha-co-regulated genes to
855 *Candida albicans* virulence. Cell Microbiol. 2005;7: 1546–1554. doi:10.1111/j.1462-
856 5822.2005.00616.x

857 11. Yue H, Bing J, Zheng Q, Zhang Y, Hu T, Du H, et al. Filamentation in *Candida auris*, an
858 emerging fungal pathogen of humans: passage through the mammalian body induces a
859 heritable phenotypic switch. Emerg Microbes Infect. 2018;7: 188. doi:10.1038/s41426-018-
860 0187-x

861 12. Bravo Ruiz G, Ross ZK, Gow NAR, Lorenz A. Pseudohyphal growth of the emerging
862 pathogen *Candida auris* is triggered by genotoxic stress through the S phase checkpoint.
863 mSphere. 2020;5: e00151-20. doi:10.1128/msphere.00151-20

864 13. Borman AM, Szekely A, Johnson EM. Comparative pathogenicity of United Kingdom
865 isolates of the emerging pathogen *Candida auris* and other key pathogenic *Candida*
866 species. mSphere. 2016;1: e00189-16. doi:10.1128/mSphere.00189-16

867 14. Santana DJ, O'Meara TR. Forward and reverse genetic dissection of morphogenesis
868 identifies filament-competent *Candida auris* strains. Nat Commun. 2021;12: 7197.
869 doi:10.1038/s41467-021-27545-5

870 15. Zamith-Miranda D, Amatuzzi RF, Munhoz da Rocha IF, Martins ST, Lucena ACR, Vieira
871 AZ, et al. Transcriptional and translational landscape of *Candida auris* in response to
872 caspofungin. Comput Struct Biotechnol J. 2021;19: 5264–5277.
873 doi:10.1016/j.csbj.2021.09.007

874 16. Szekely A, Borman AM, Johnson EM. *Candida auris* isolates of the Southern Asian and
875 South African lineages exhibit different phenotypic and antifungal susceptibility profiles *in*
876 *vitro*. J Clin Microbiol. 2019;57: e02055-18. doi:10.1128/jcm.02055-18

877 17. Bing J, Guan Z, Zheng T, Zhang Z, Fan S, Ennis CL, et al. Clinical isolates of *Candida*
878 *auris* with enhanced adherence and biofilm formation due to genomic amplification of
879 *ALS4*. PLoS Pathog. 2023;19: e1011239. doi:10.1371/journal.ppat.1011239

880 18. Forgács L, Borman AM, Prépost E, Tóth Z, Kovács R, Szekely A, et al. Comparison of *in*
881 *vivo* pathogenicity of four *Candida auris* clades in a neutropenic bloodstream infection
882 murine model. Emerg Infect Dis. 2020;9: 1160–1169. doi:10.1080/22221751.2020.1771218

883 19. Bravo Ruiz G, Lorenz A. What do we know about the biology of the emerging fungal
884 pathogen of humans *Candida auris*? Microbiol Res. 2021;242: 126621.
885 doi:10.1016/j.micres.2020.126621

886 20. Malavia-Jones D, Farrer RA, Stappers MHT, Edmondson MB, Borman AM, Johnson EM,
887 et al. Strain and temperature dependent aggregation of *Candida auris* is attenuated by
888 inhibition of surface amyloid proteins. The Cell Surface. 2023;10: 100110.
889 doi:10.1016/j.tcsw.2023.100110

890 21. Ramos LS, Parra-Giraldo CM, Branquinha MH, Santos ALS. Cell aggregation capability of
891 clinical isolates from *Candida auris* and *Candida haemulonii* species complex. Trop Med
892 Infect Dis. 2023;8: 382. doi:10.3390/tropicalmed8080382

893 22. Short B, Brown J, Delaney C, Sherry L, Williams C, Ramage G, et al. *Candida auris*
894 exhibits resilient biofilm characteristics *in vitro*: implications for environmental persistence.
895 Journal of Hospital Infection. 2019;103: 92–96. doi:10.1016/j.jhin.2019.06.006

896 23. Singh R, Kaur M, Chakrabarti A, Shankarnarayan SA, Rudramurthy SM. Biofilm formation
897 by *Candida auris* isolated from colonising sites and candidemia cases. Mycoses. 2019;62:
898 706–709. doi:10.1111/myc.12947

899 24. Romera D, Aguilera-Correa J-J, García-Coca M, Mahillo-Fernández I, Viñuela-Sandoval L,
900 García-Rodríguez J, et al. The *Galleria mellonella* infection model as a system to
901 investigate the virulence of *Candida auris* strains. Pathog Dis. 2020;78: ftaa067.
902 doi:10.1093/femspd/ftaa067

903 25. Biswas B, Gangwar G, Nain V, Gupta I, Thakur A, Puria R. Rapamycin and Torin2 inhibit
904 *Candida auris* TOR: Insights through growth profiling, docking, and MD simulations. J
905 Biomol Struct Dyn. 2022. doi:10.1080/07391102.2022.2134927

906 26. Hoyer LL, Cota E. *Candida albicans* Agglutinin-like sequence (Als) family vignettes: a
907 review of Als protein structure and function. Front Microbiol. 2016;7: 280.
908 doi:10.3389/fmicb.2016.00280

909 27. Muñoz JF, Gade L, Chow NA, Loparev VN, Juieng P, Berkow EL, et al. Genomic insights
910 into multidrug-resistance, mating and virulence in *Candida auris* and related emerging
911 species. Nat Commun. 2018;9: 5346. doi:10.1038/s41467-018-07779-6

912 28. Muñoz JF, Welsh RM, Shea T, Batra D, Gade L, Howard D, et al. Clade-specific
913 chromosomal rearrangements and loss of subtelomeric adhesins in *Candida auris*.
914 Genetics. 2021;218: iyab029. doi:10.1093/genetics/iyab029

915 29. Singh S, Uppuluri P, Mamouei Z, Alqarihi A, Elhassan H, French S, et al. The NDV-3A
916 vaccine protects mice from multidrug resistant *Candida auris* infection. PLoS Pathog.
917 2019;15: e1007460. doi:10.1371/journal.ppat.1007460

918 30. Smoak RA, Snyder LF, Fassler JS, He BZ. Parallel expansion and divergence of an
919 adhesin family in pathogenic yeasts. Genetics. 2023;223: iyad024.
920 doi:10.1093/genetics/iyad024

921 31. Santana DJ, Anku JAE, Zhao G, Zarnowski R, Johnson CJ, Hautau H, et al. A *Candida*
922 *auris* –specific adhesin, Scf1, governs surface association, colonization, and virulence.
923 Science. 2023;381: 1461–1467. doi:10.1126/science.adf8972

924 32. Liu Y, Filler SG. *Candida albicans* Als3, a multifunctional adhesin and invasin. Eukaryot
925 Cell. 2011;10: 168–173. doi:10.1128/EC.00279-10

926 33. Willaert R. Adhesins of yeasts: protein structure and interactions. Journal of Fungi. 2018;4:
927 119. doi:10.3390/jof4040119

928 34. Mayr E-M, Ramírez-Zavala B, Krüger I, Morschhäuser J. A Zinc Cluster transcription factor
929 contributes to the intrinsic fluconazole resistance of *Candida auris*. mSphere. 2020;5:
930 e00279-20. doi:10.1128/mSphere.00279-20

931 35. Garcia-Bustos V, Ruiz-Saurí A, Ruiz-Gaitán A, Sigona-Giangreco IA, Cabañero-Navalon
932 MD, Sabalza-Baztán O, et al. Characterization of the differential pathogenicity of *Candida*
933 *auris* in a *Galleria mellonella* infection model. Microbiol Spectr. 2021;9: e00013-21.
934 doi:10.1128/Spectrum.00013-21

935 36. Ene I V., Adya AK, Wehmeier S, Brand AC, MacCallum DM, Gow NAR, et al. Host carbon
936 sources modulate cell wall architecture, drug resistance and virulence in a fungal
937 pathogen. Cell Microbiol. 2012;14: 1319–1335. doi:10.1111/j.1462-5822.2012.01813.x

938 37. Leach MD, Farrer RA, Tan K, Miao Z, Walker LA, Cuomo CA, et al. Hsf1 and Hsp90
939 orchestrate temperature-dependent global transcriptional remodelling and chromatin
940 architecture in *Candida albicans*. Nat Commun. 2016;7: 11704. doi:10.1038/ncomms11704

941 38. Thompson DS, Carlisle PL, Kadosh D. Coevolution of morphology and virulence in
942 *Candida* species. Eukaryot Cell. 2011;10: 1173–1182. doi:10.1128/EC.05085-11

943 39. Brown AJP, Brown GD, Netea MG, Gow NAR. Metabolism impacts upon *Candida*
944 immunogenicity and pathogenicity at multiple levels. Trends Microbiol. 2014;22: 614–622.
945 doi:10.1016/j.tim.2014.07.001

946 40. Lorenz A, Papon N. New tools for the new bug *Candida auris*. Trends Microbiol. 2022;30:
947 203–205. doi:10.1016/j.tim.2022.01.010

948 41. Wang Y, Zou Y, Chen X, Li H, Yin Z, Zhang B, et al. Innate immune responses against the
949 fungal pathogen *Candida auris*. Nat Commun. 2022;13: 3553. doi:10.1038/s41467-022-
950 31201-x

951 42. Milne G, Walker LA. High-pressure freezing and transmission electron microscopy to
952 visualize the ultrastructure of the *C. auris* cell wall. Methods in Molecular Biology.
953 2022;2517: 189–201. doi:10.1007/978-1-0716-2417-3_15

954 43. Schindelin J, Arganda-Carreras I, Frise E, Kaynig V, Longair M, Pietzsch T, et al. Fiji: an
955 open-source platform for biological-image analysis. Nat Methods. 2012;9: 676–682.
956 doi:10.1038/nmeth.2019

957 44. The External RNA Controls Consortium. The External RNA Controls Consortium: a
958 progress report. Nat Methods. 2005;2: 731–734. doi:10.1038/nmeth1005-731

959 45. Kim D, Langmead B, Salzberg SL. HISAT: a fast spliced aligner with low memory
960 requirements. Nat Methods. 2015;12: 357–360. doi:10.1038/nmeth.3317

961 46. Chatterjee S, Alampalli SV, Nageshan RK, Chettiar ST, Joshi S, Tatu US. Draft genome of
962 a commonly misdiagnosed multidrug resistant pathogen *Candida auris*. BMC Genomics.
963 2015;16: 686. doi:10.1186/s12864-015-1863-z

964 47. Li H, Handsaker B, Wysoker A, Fennell T, Ruan J, Homer N, et al. The Sequence
965 Alignment/Map format and SAMtools. Bioinformatics. 2009;25: 2078–2079.
966 doi:10.1093/bioinformatics/btp352

967 48. Liao Y, Smyth GK, Shi W. featureCounts: an efficient general purpose program for
968 assigning sequence reads to genomic features. Bioinformatics. 2014;30: 923–930.
969 doi:10.1093/bioinformatics/btt656

970 49. Robinson MD, McCarthy DJ, Smyth GK. edgeR: a Bioconductor package for differential
971 expression analysis of digital gene expression data. Bioinformatics. 2010;26: 139–140.
972 doi:10.1093/bioinformatics/btp616

973 50. Camacho C, Coulouris G, Avagyan V, Ma N, Papadopoulos J, Bealer K, et al. BLAST+:
974 architecture and applications. BMC Bioinformatics. 2009;10: 421. doi:10.1186/1471-2105-
975 10-421

976 51. Bravo Ruiz G, Lorenz A. Genetic transformation of *Candida auris* via homology-directed
977 repair using a standard lithium acetate protocol. Methods in Molecular Biology. 2022;2517:
978 95–110. doi:10.1007/978-1-0716-2417-3_8

979 52. Daigneault M, Preston JA, Marriott HM, Whyte MKB, Dockrell DH. The identification of
980 markers of macrophage differentiation in PMA-stimulated THP-1 cells and monocyte-
981 derived macrophages. PLoS One. 2010;5: e8668. doi:10.1371/journal.pone.0008668

982

983

984